

# Reconstructing dynamics from sparse observations with no training on target system

Zheng-Meng Zhai,<sup>1</sup> Jun-Yin Huang,<sup>1</sup> Benjamin D. Stern,<sup>2</sup> and Ying-Cheng Lai<sup>1,3,\*</sup>

<sup>1</sup>*School of Electrical, Computer and Energy Engineering,  
Arizona State University, Tempe, AZ 85287, USA*

<sup>2</sup>*Doctor of Physical Therapy Program, Tufts University School of Medicine,  
101 E Washington St Suite 950, Phoenix, AZ 85004, USA*

<sup>3</sup>*Department of Physics, Arizona State University, Tempe, Arizona 85287, USA*

(Dated: October 29, 2024)

In applications, an anticipated situation is where the system of interest has never been encountered before and sparse observations can be made only once. Can the dynamics be faithfully reconstructed from the limited observations without any training data? This problem defies any known traditional methods of nonlinear time-series analysis as well as existing machine-learning methods that typically require extensive data from the target system for training. We address this challenge by developing a hybrid transformer and reservoir-computing machine-learning scheme. The key idea is that, for a complex and nonlinear target system, the training of the transformer can be conducted not using any data from the target system, but with essentially unlimited synthetic data from known chaotic systems. The trained transformer is then tested with the sparse data from the target system. The output of the transformer is further fed into a reservoir computer for predicting the long-term dynamics or the attractor of the target system. The power of the proposed hybrid machine-learning framework is demonstrated using a large number of prototypical nonlinear dynamical systems, with high reconstruction accuracy even when the available data is only 20% of that required to faithfully represent the dynamical behavior of the underlying system. The framework provides a paradigm of reconstructing complex and nonlinear dynamics in the extreme situation where training data does not exist and the observations are random and sparse.

## I. INTRODUCTION

In applications of complex systems, observations are fundamental to tasks such as mechanistic understanding, dynamics reconstruction, state prediction, and control. When the available data are complete in the sense that the data points are sampled according to the Nyquist criterion and no points are missing, it is possible to extract the dynamics or even find the equations of the system from data by sparse optimization [1, 2]. In machine learning, reservoir computing has been widely applied to complex and nonlinear dynamical systems for tasks such as prediction [3–27], control [28], signal detection [29], and estimation [30]. Quite recently, Kolmogorov-Arnold networks (KANs) [31], typically small neural networks, were proposed for discovering the dynamics from data, where even symbolic regression is possible in some cases to identify the exact mathematical equations and parameters. It has also been demonstrated [32] that the KANs have the power of uncovering the dynamical system in situations where the methods of sparse optimization fail. In all these applications, an essential requirement is that the time-series data are complete in the Nyquist sense.

A challenging but not uncommon situation is where a new system is to be learned and eventually controlled based on limited observations. Two significant difficulties arise in this case. First, being “new” means that the system has not been observed before, so no previous data or recordings exist. If one intends to exploit machine

learning to learn and reconstruct the dynamics of the system from observations, no training data are available. Second, the observations may be irregular and sparse: the observed data are not collected at some uniform time interval, e.g., as determined by the Nyquist criterion, but at random times with the total data amount much less than that from Nyquist sampling. It is also possible that the observations can be made only once. The question is, provided with one-time sparse observations or time-series data, can the dynamics of the underlying system still be faithfully reconstructed?

Limited observations or data occur in various real-world situations. For example, ecological data gathered from diverse and dynamic environments inevitably contain gaps caused by equipment failure, weather conditions, limited access to remote locations, and temporal or financial constraints. Similarly, in medical systems and human activity tracking, data collection frequently suffers from issues such as patient noncompliance, recording errors, loss of followup, and technical failures. Wearable devices present additional challenges, including battery depletion, user error, signal interference from clothing or environmental factors, and inconsistent wear patterns during sleep or specific activities where devices may need to be removed. A common feature of these scenarios is that the available data are only from random times without any discernible patterns. This issue becomes particularly problematic when the data is sparse. Being able to reconstruct the dynamics from sparse and random data is particularly challenging for nonlinear dynamical systems due to the possibility of chaos leading to a sensitive dependence on small errors. For example, large errors

---

\* Ying-Cheng.Lai@asu.edu

may arise when predicting the values of the dynamical variables in various intervals in which data are missing. However, if training data from the *same* target system are available, machine learning can be effective for reconstructing the dynamics from sparse data [33]. (Additional background on machine-learning approaches is provided in Appendix A.)

It is necessary to define what we mean by “random and sparse” data. We consider systems whose dynamics occur within certain finite frequency band. For chaotic systems with a broad power spectrum, in principle the “cutoff” frequency can be arbitrarily large, but power contained in a frequency range near and beyond the cutoff frequency can often be significantly smaller than that in the low frequency domain and thus can be neglected, leading realistically to a finite yet still large bandwidth. A meaningful Nyquist sampling frequency can then be defined. An observational dataset being complete means that the time series are recorded at the *regular* time interval as determined by the Nyquist frequency with no missing points. In this case, the original signal can be faithfully reconstructed. Random and sparse data mean that the data points are sampled at *irregular* time intervals and some portion of the data points as determined by the Nyquist frequency are missing at random times. We aim to reconstruct the system dynamics from random and sparse observations by developing a machine-learning framework to generate continuous time series that meet the Nyquist criteria, i.e., time series represented by regularly sampled data points of frequency at or exceeding the Nyquist frequency. When the governing equations of the underlying system are unknown and/or when historical observations of the full dynamical trajectory of the system are not available, the resulting lack of any training data makes the reconstruction task extremely challenging. Indeed, since the system cannot be fully measured and only irregularly observed data points are available, directly inferring the dynamical trajectory from these points is infeasible. Furthermore, the extent of the available observed data points and the number of data points to be interpolated can be uncertain.

In this paper, we develop a machine-learning framework to address the problem of dynamics reconstruction and prediction from random and sparse observations with no training data from the target system. Our key innovation is training a hybrid machine-learning framework in a laboratory environment using a variety of synthetic dynamical systems other than data from the target system itself, and deploy the trained architecture to reconstruct the dynamics of the target system from one-time sparse observations. More specifically, we exploit the machine-learning framework of transformers with training data *not from the target system* but from a number of known, synthetic systems that show qualitatively similar dynamical behaviors to those of the target system, for which complete data are available. The training process can thus be regarded as a “laboratory-calibration” process during which the transformer learns the dynamical

rules generating the synthetic but complete data. The so-trained transformer is then deployed to the real application with the random and sparse data, and is expected to adapt to the unseen data and reconstruct the underlying dynamics. To enable long-term prediction of the target system, we exploit reservoir computing that has been demonstrated to be particularly suitable for predicting nonlinear dynamics [3–27] by feeding the output of the transformer into the reservoir computer. This combination of transformer and reservoir computing constitutes a hybrid machine-learning framework. We demonstrate that it can successfully reconstruct the dynamics of approximately three dozen prototypical nonlinear systems, with high reconstruction accuracy even when the available data is only 20% of that required to faithfully represent the dynamical behavior of the underlying system according to the Nyquist criterion. Our framework provides a paradigm of reconstructing complex and nonlinear dynamics in the extreme situation where training data from the target system do not exist and the observations or measurements are severely insufficient.

## II. HYBRID MACHINE LEARNING

Figure 1 highlights the challenge of reconstructing the dynamics from sparse data without training data. In particular, Fig. 1(a) shows the textbook case of a random time series sampled at a frequency higher than the Nyquist frequency, which can be completely reconstructed. To illustrate random and sparse data in an intuitive setting, we consider a set of six available data points from a unit time interval, as shown in Figs. 1(b) and 1(c). The time interval contains approximately two periods of oscillation, which defines a local frequency denoted as  $f_{\text{local}} = 2$ . As the signal is chaotic or random, the cutoff frequency  $f_{\text{max}}$  in the power spectrum can be higher than the frequency represented by the two oscillation cycles as shown. As a concrete example, we assume  $f_{\text{max}} = 5f_{\text{local}}$ , so the Nyquist frequency is  $f_{\text{Nyquist}} = 10f_{\text{local}}$ . If the signal is sampled at the corresponding Nyquist time interval  $\Delta T = 1/f_{\text{Nyquist}} = 1/20$ , 20 data points would be needed. If these 20 points are sampled uniformly in time, then the signal in the two oscillation cycles can be reconstructed. The reconstruction becomes quite challenging due to two factors: the limited availability of only six data points and their random distribution across the unit time interval. Consider points #5 and #6, which occur during a downward oscillation cycle in the ground truth data. Accurately reconstructing this downward oscillation presents a key challenge. When training data from the same target system is available, standard machine learning techniques can faithfully reconstruct the dynamics [33], as demonstrated in Fig. 1(b). However, without access to training data from the target system, previous methods were unable to reconstruct the dynamics from such sparse observations. A related question is, after the reconstruction,

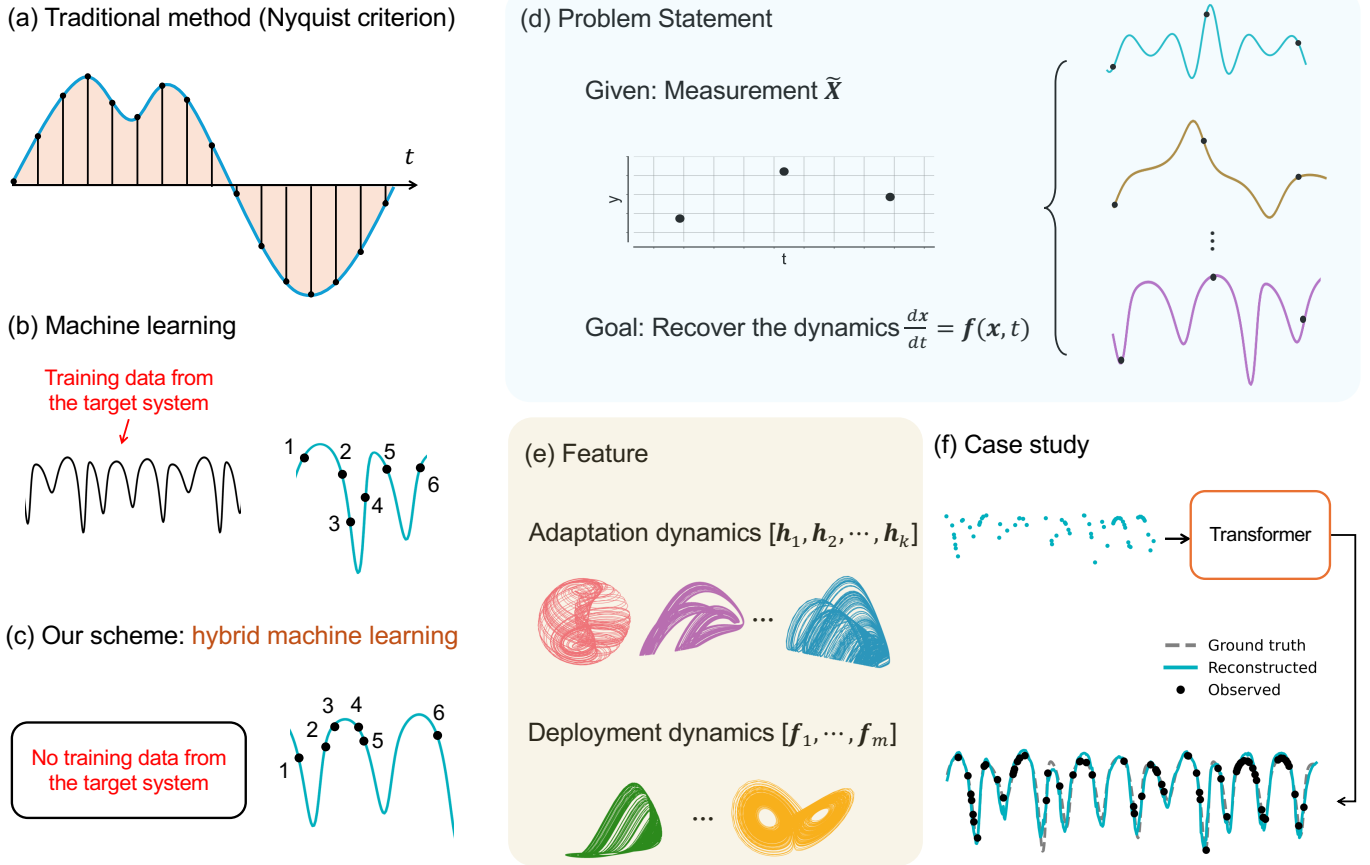


FIG. 1. Dynamics reconstruction from random and sparse data. (a) The textbook case of a random time series sampled at a frequency higher than the Nyquist frequency, where the dynamical data can be faithfully reconstructed. (b) Training data from the target system (left) and a segment of time series of six data points in a time interval containing approximately two cycles of oscillation. According to the Nyquist criterion, the signal can be faithfully reconstructed with more than 20 uniformly sampled data points (see text). When the data points are far fewer than 20 and even worse, they are randomly sampled, reconstruction becomes challenging. However, if training data from the same target system are available, existing machine-learning methods can be used to reconstruct the dynamics from the sparse data [33]. (c) If no training data from the target system are available, hybrid machine learning proposed here provides a viable solution to reconstructing the dynamics from sparse data. (d) Problem statement. Given random and sparse data, the goal is to reconstruct the dynamics of the target system governed by  $dx/dt = f(x, t)$ . A hurdle that needs to be overcome is that, for any given three points, there exist infinitely many ways to fit the data, as illustrated on the right side. (e) Training of the machine-learning framework is done using complete data from a large number of synthetic dynamical systems  $[h_1, h_2, \dots, h_k]$ . The framework is then adapted to reconstruct and predict the dynamics of the target systems  $[f_1, \dots, f_m]$ . (f) An example: in the testing (deployment) phase, sparse observations are provided to the trained neural network for dynamics reconstruction.

can the long-term dynamics or attractor of the system be predicted? We shall demonstrate that both the reconstruction and long-term prediction problems can be solved with hybrid machine learning, as schematically illustrated in Figs. 1(d-f).

Consider a nonlinear dynamical system described by

$$\frac{d\mathbf{x}(t)}{dt} = \mathbf{f}(\mathbf{x}(t), t), \quad t \in [0, T], \quad (1)$$

where  $\mathbf{x}(t) \in \mathbb{R}^D$  is a  $D$ -dimensional state vector and  $\mathbf{f}(\cdot)$  is the unknown velocity field. Let  $\mathbf{X} = (\mathbf{x}_0, \dots, \mathbf{x}_{L_s})^\top \in \mathbb{R}^{L_s \times D}$  be the full uniformly sampled data matrix of dimension  $L_s \times D$  with each dimension of the original dy-

namical variable containing  $L_s$  points. A sparse observational vector can be expressed as

$$\tilde{\mathbf{X}} = \mathbf{g}_\alpha(\mathbf{X})(1 + \sigma \cdot \Xi), \quad (2)$$

where  $\tilde{\mathbf{X}} \in \mathbb{R}^{L_s \times D}$  is the observational data matrix of dimension  $L_s \times D$  and  $\mathbf{g}_\alpha(\cdot)$  is the following element-wise observation function:

$$X_{ij}^O = g_\alpha(X_{ij}) = \begin{cases} X_{ij}, & \text{if } X_{ij} \text{ is observed,} \\ 0, & \text{otherwise,} \end{cases} \quad (3)$$

with  $\alpha$  representing the probability of matrix element  $X_{ij}$  being observed. In Eq. (2), Gaussian white noise

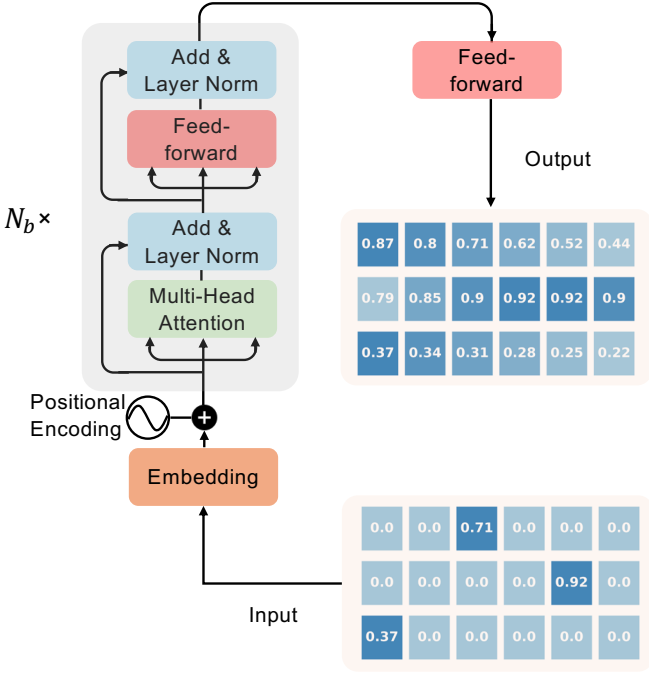


FIG. 2. Transformer architecture. The transformer receives the sparse and random observation as the input and generates the reconstructed output. See text for a detailed mathematical description.

of amplitude  $\sigma$  is present during the measurement process, where  $\Xi \sim \mathcal{N}(0, 1)$ . Our goal is utilizing machine learning to approximate the system dynamics function  $\mathbf{f}(\cdot)$  by another function  $\mathbf{f}'(\cdot)$ , assuming that  $\mathbf{f}$  is Lipschitz continuous with respect to  $\mathbf{x}$  and the observation function produces sparse data:  $\mathbf{g} : \mathbf{X} \rightarrow \tilde{\mathbf{X}}$ . To achieve this, it is necessary to design a function  $\mathcal{F}(\tilde{\mathbf{X}}) = \mathbf{X}$  that comprises implicitly  $\mathbf{f}'(\cdot) \approx \mathbf{f}(\cdot)$  so that it recovers the system dynamics by filling the gaps in the observation, where  $\mathcal{F}(\tilde{\mathbf{X}})$  should have the capability of adapting to any given unknown dynamics.

Selecting an appropriate neural network architecture for reconstructing dynamics from sparse data requires meeting two fundamental requirements: (1) dynamical memory to capture long-range dependencies in the sparse data, and (2) flexibility to handle input sequences of varying lengths. Transformers [34], originally developed for natural language processing, satisfy these requirements and have proven effective for time series analysis. Figure 2 illustrates the transformer's main structure. The data matrix  $\tilde{\mathbf{X}}$  is first processed through a linear fully-connected layer with bias, transforming it into an  $L_s \times N$  matrix. This output is then combined with a positional encoding matrix, which embeds temporal ordering information into the time series data. This projection process can be described as [35]:

$$\mathbf{X}_p = \tilde{\mathbf{X}}\mathbf{W}_p + \mathbf{W}_b + \mathbf{PE}, \quad (4)$$

where  $\mathbf{W}_p \in \mathbb{R}^{D \times N}$  represents the fully-connected layer

with the bias matrix  $\mathbf{W}_b \in \mathbb{R}^{L_s \times N}$  and the position encoding matrix is  $\mathbf{PE} \in \mathbb{R}^{L_s \times N}$ . Since the transformer model does not inherently capture the order of the input sequence, positional encoding is necessary to provide the information about the position of each time step. For a given position  $1 \leq \text{pos} \leq L_s^{\max}$  and dimension  $1 \leq d \leq D$ , the encoding is given by

$$\mathbf{PE}_{\text{pos}, 2d} = \sin\left(\frac{\text{pos}}{10000^{2d/N}}\right), \quad (5)$$

$$\mathbf{PE}_{\text{pos}, 2d+1} = \cos\left(\frac{\text{pos}}{10000^{2d/N}}\right), \quad (6)$$

The projected matrix  $\mathbf{X}_p \in \mathbb{R}^{L_s \times N}$  then serves as the input sequence for  $N_b$  attention blocks. Each block contains a multi-head attention layer, a residual layer (add & layer norm), and a feed-forward layer, and a second residual layer. The core of the transformer lies in the self-attention mechanism, allowing the model to weight the significance of distinct time steps. The multi-head self-attention layer is composed of several independent attention blocks. The first block has three learnable weight matrices that linearly map  $\mathbf{X}_p$  into query  $\mathbf{Q}_1$  and key  $\mathbf{K}_1$  of the dimension  $L_s \times d_k$  and value  $\mathbf{V}_1$  of the dimension  $L_s \times d_v$ :

$$\mathbf{Q}_1 = \mathbf{X}_p\mathbf{W}_{\mathbf{Q}_1}, \quad \mathbf{K}_1 = \mathbf{X}_p\mathbf{W}_{\mathbf{K}_1}, \quad \mathbf{V}_1 = \mathbf{X}_p\mathbf{W}_{\mathbf{V}_1}, \quad (7)$$

where  $\mathbf{W}_{\mathbf{Q}_1} \in \mathbb{R}^{N \times d_k}$ ,  $\mathbf{W}_{\mathbf{K}_1} \in \mathbb{R}^{N \times d_k}$ , and  $\mathbf{W}_{\mathbf{V}_1} \in \mathbb{R}^{N \times d_v}$  are the trainable weight matrices,  $d_k$  is the dimension of the queries and keys, and  $d_v$  is the dimension of the values. A convenient choice is  $d_k = d_v = N$ . The attention scores between the query  $\mathbf{Q}_1$  and the key  $\mathbf{K}_1$  are calculated by a scaled multiplication, followed by a softmax function:

$$\mathbf{A}_{\mathbf{Q}_1, \mathbf{K}_1} = \text{softmax}\left(\frac{\mathbf{Q}_1\mathbf{K}_1^T}{\sqrt{d_k}}\right), \quad (8)$$

where  $\mathbf{A}_{\mathbf{Q}_1, \mathbf{K}_1} \in \mathbb{R}^{L_s \times L_s}$ . The softmax function normalizes the data with  $\text{softmax}(x_i) = \exp(x_i) / \sum_j \exp(x_j)$ , and the  $\sqrt{d_k}$  factor mitigates the enlargement of standard deviation due to matrix multiplication. For the first head (in the first block), the attention matrix is computed as a dot product between  $\mathbf{A}_{\mathbf{Q}_1, \mathbf{K}_1}$  and  $\mathbf{V}_1$ :

$$\begin{aligned} \mathbf{O}_{11} &= \text{Attention}(\mathbf{Q}_1, \mathbf{K}_1, \mathbf{V}_1), \\ &= \mathbf{A}_{\mathbf{Q}_1, \mathbf{K}_1}\mathbf{V}_1 = \text{softmax}\left(\frac{\mathbf{Q}_1\mathbf{K}_1^T}{\sqrt{d_k}}\right)\mathbf{V}_1, \end{aligned} \quad (9)$$

where  $\mathbf{O}_{11} \in \mathbb{R}^{L_s \times d_v}$ . The transformer employs multiple ( $h$ ) attention heads to capture information from different subspaces. The resulting attention heads  $\mathbf{O}_{1i}$  ( $i = 1, \dots, h$ ) are concatenated and mapped into a sequence  $\mathbf{O}_1 \in \mathbb{R}^{L_s \times N}$ , described as:

$$\mathbf{O}_1 = \mathcal{C}(\mathbf{O}_{11}, \mathbf{O}_{12}, \dots, \mathbf{O}_{1h})\mathbf{W}_{\mathbf{O}_1}, \quad (10)$$

where  $\mathcal{C}$  is the concatenation operation,  $h$  is the number of heads, and  $\mathbf{W}_{\mathbf{O}_1} \in \mathbb{R}^{hd_v \times N}$  is an additional matrix

for linear transformation for performance enhancement. The output of the attention layer undergoes a residual connection and layer normalization, producing  $\mathbf{X}_{R1}$  as follows:

$$\mathbf{X}_{R1} = \text{LayerNorm}(\mathbf{X}_p + \text{Dropout}(\mathbf{O}_1)) \quad (11)$$

A feed-forward layer then processes this data matrix, generating output  $\mathbf{X}_{F1} \in \mathbb{R}^{L_s \times N}$  as:

$$\mathbf{X}_{F1} = \max(0, \mathbf{X}_{R1} \mathbf{W}_{F_a} + \mathbf{b}_a) \mathbf{W}_{F_b} + \mathbf{b}_b, \quad (12)$$

where  $\mathbf{W}_{F_a} \in \mathbb{R}^{N \times d_f}$ ,  $\mathbf{W}_{F_b} \in \mathbb{R}^{d_f \times N}$ ,  $\mathbf{b}_a$  and  $\mathbf{b}_b$  are biases, and  $\max(0, \cdot)$  denotes a ReLU activation function. This output is again subjected to a residual connection and layer normalization.

The output of the first block operation is used as the input to the second block. The same procedure is repeated for each of the remaining  $N_b - 1$  blocks. The final output passes through a feed-forward layer to generate the prediction. Overall, the whole process can be represented as  $\mathbf{Y} = \mathcal{F}(\tilde{\mathbf{X}})$ .

To evaluate the reliability of the generated output, we minimize a combined loss function with two components: (1) a mean squared error (MSE) loss that measures absolute error between the output and ground truth, and (2) a smoothness loss that ensures the output maintains appropriate continuity. The loss function is given by

$$\mathcal{L} = \alpha_1 \mathcal{L}_{\text{mse}} + \alpha_2 \mathcal{L}_{\text{smooth}}, \quad (13)$$

where  $\alpha_1$  and  $\alpha_2$  are scalar weights controlling the trade-off between the two loss terms. The first component  $\mathcal{L}_{\text{mse}}$  measures the absolute error between the predictions and the ground truth:

$$\mathcal{L}_{\text{mse}} = \frac{1}{n} \sum_{i=1}^n (y_i - \hat{y}_i)^2, \quad (14)$$

with  $n$  being the total number of data points,  $y_i$  and  $\hat{y}_i$  denoting the ground truth and predicted value at time point  $i$ , respectively. The second component  $\mathcal{L}_{\text{smooth}}$  of the loss function consists of two terms: Laplacian regularization and total variation regularization, which penalize the second-order differences and absolute differences, respectively, between consecutive predictions. The two terms are given by:

$$\mathcal{L}_{\text{laplacian}} = \frac{1}{n-2} \sum_{i=2}^{n-1} (\hat{y}_{i-1} + \hat{y}_{i+1} - 2\hat{y}_i)^2, \quad (15)$$

and

$$\mathcal{L}_{\text{tv}} = \frac{1}{n-1} \sum_{i=1}^{n-1} |\hat{y}_i - \hat{y}_{i+1}|. \quad (16)$$

We assign the same weights to the two penalties, so the final combined loss function to be minimized is

$$\mathcal{L} = \mathcal{L}_{\text{mse}} + \alpha_s (\mathcal{L}_{\text{laplacian}} + \mathcal{L}_{\text{tv}}). \quad (17)$$

We set  $\alpha_s = 0.1$ .

The second component of our hybrid machine-learning framework is reservoir computing, which takes the output of the transformer as the input to reconstruct the long-term ‘‘climate’’ or attractor of the target system. A detailed description of reservoir computing used in this context and its hyperparameters optimization are presented in Appendices C and D.

### III. RESULTS

We test our approach on three nonlinear dynamical systems in the deployment phase: a three-species chaotic food chain system [36], the classic chaotic Lorenz system [37], and Lotka-Volterra system [38]. The transformer had no prior exposure to these systems during its training (adaptation) phase. We use sparse observational data from each system to reconstruct their underlying dynamics.

In the training phase, 28 synthetic chaotic systems are used to train the transformer, enabling it to learn to extract dynamic behaviors from sparse observations (see Appendix B for a detailed description). To enable the transformer to handle data from new, unseen systems of arbitrary time series length  $L_s$  and sparsity  $S_r$ , we employ the following strategy at each training step: (1) randomly selecting a system from the pool of synthetic chaotic systems and (2) preprocessing the data from the system using a uniformly distributed time series length  $L_s \sim U(1, L_s^{\text{max}})$ , and uniformly distributed sparsity  $S_r \sim U(0, 1)$ . By so doing, we prevent the transformer from learning any specific system dynamics too well, thereby encouraging it to treat each set of inputs as a new system. In addition, the strategy teaches the transformer to master as many features as possible. Figure 3(a) illustrates the training phase, with examples shown on the left side. On the right side, the sampled examples are encoded and fed into the transformer. The performance is evaluated by MSE loss and smoothness loss between the output and ground truth, and is used to

TABLE I. Optimal transformer hyperparameter values

Hyperparameters	Descriptions
$D_l = 1, 500, 000$	Training length for each system
$d_f = 512$	Number of Feedforward neurons
$h = 4$	Number of Transformer heads
$N_b = 4$	Number of Transformer blocks
$N = 128$	input embedded dimension
$\sigma = 0.05$	Measurement noise level
$L_s^{\text{max}} = 3000$	Maximum input sequence length
$b_s = 16$	Batch size
epoch = 50	Epoch
$lr = 0.001$	Learning rate
$P_{\text{drop}} = 0.2$	Dropout rate

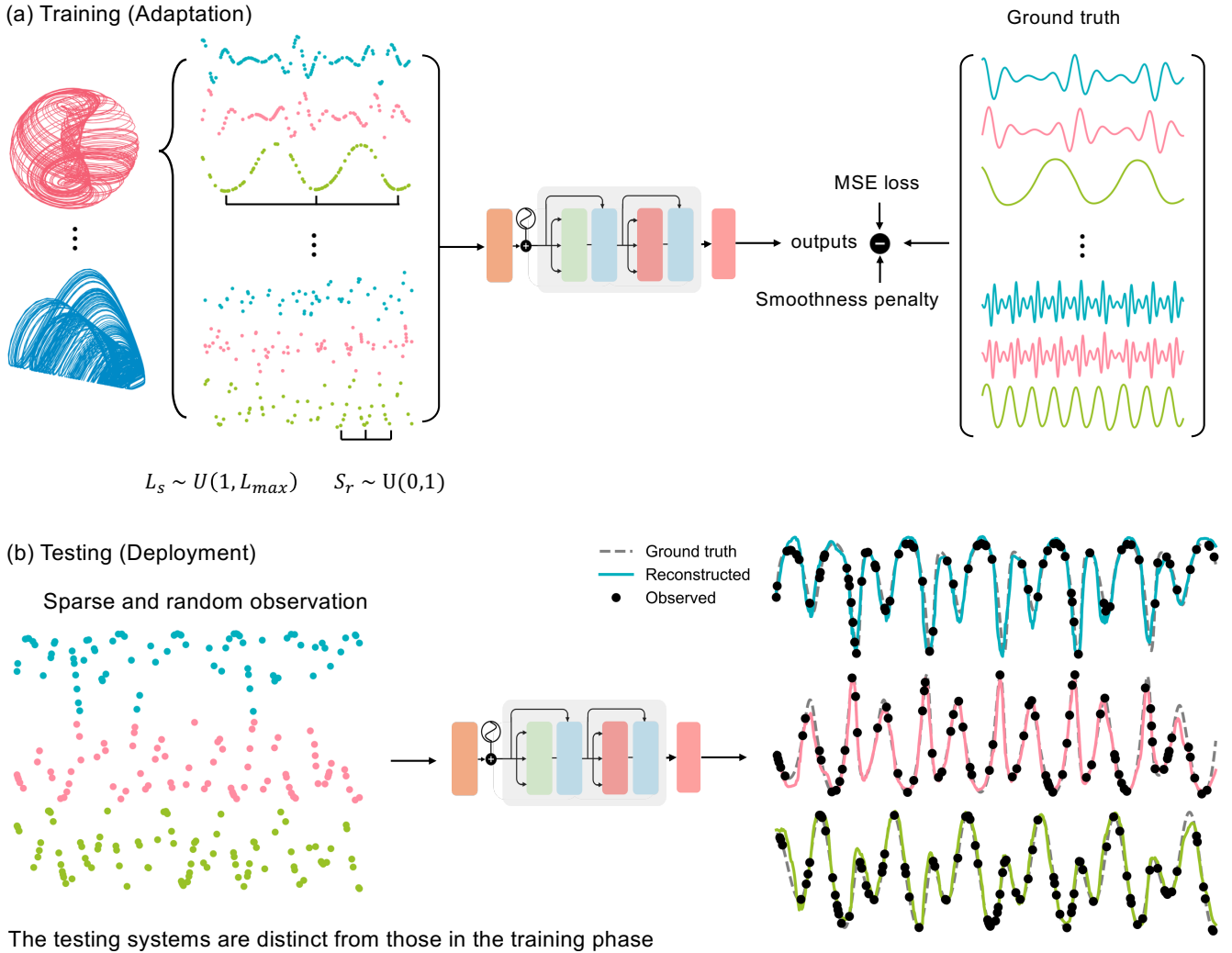


FIG. 3. Illustration of the transformer-based dynamics reconstruction framework. (a) Training (adaptation) phase, where the model is trained on various synthetic chaotic systems, each divided into segments with randomly distributed sequence lengths  $L_s$  and sparsity  $S_r$ . The data is masked before being input into the transformer, and the ground truth is used to minimize the MSE loss and smoothness loss with the output. By learning a randomly chosen segment from a random training system each time, the transformer is trained to handle data with varying lengths and different levels of sparsity. (b) Testing (deployment) phase. The testing systems are distinct from those in the training phase, i.e., the transformer is not trained on any of the testing systems. Given sparsely observed set of points, the transformer is able to reconstruct the dynamical trajectory.

update the neural-network weights.

Unless otherwise stated, the following computational settings for machine learning are used. Given a target system, time series are generated numerically by integrating the system with time step  $dt = 0.01$ . The initial states of both the dynamical process and the neural network are randomly set from a uniform distribution. An initial phase of the time series is removed to ensure that the trajectory has reached the attractor. The training and testing data are obtained by sampling the time series at the interval  $\Delta_s$  chosen to ensure an acceptable generation. Specifically, for the chaotic food chain, Lorenz and Lotka-Volterra systems, we set  $\Delta_s = 10dt = 0.1$ , corresponding to approximately 1 over 40  $\sim$  50 cycles of oscillation. A similar procedure is also applied to other

synthetic chaotic systems. The time series data are pre-processed by using min-max normalization so that they are in the range  $[0,1]$ . The complete data length for each system is 1,500,000 (about 30,000 cycles of oscillations), which is divided into segments with randomly chosen sequence lengths  $L_s$  and sparsity  $S_r$ . For the transformer, we use a maximum sequence length of 3,000 (corresponding to about 60 cycles of oscillations) - the limitation of input time series length. We apply Bayesian optimization [39] and a random search algorithm [40] to systematically explore and identify the optimal set of various hyperparameters. Two chaotic Sprott systems - Sprott<sub>0</sub> and Sprott<sub>1</sub> - are used to find the optimal hyperparameters, ensuring no data leakage from the testing systems. The optimized hyperparameters for the transformer are

listed in Table I. Simulations are run using Python on computers with six RTX A6000 NVIDIA GPUs.

For clarity of presentation, in the main text, we focus on the results from the chaotic three-species food-chain system, while leaving the results from the other two testing systems in Appendix E.

### A. Dynamics reconstruction

The three species food-chain system [36] is described by

$$\begin{aligned} \frac{dR}{dt} &= R\left(1 - \frac{R}{K}\right) - \frac{x_c y_c CR}{R + R_0}, \\ \frac{dC}{dt} &= x_c C \left(\frac{y_c R}{R + R_0} - 1\right) - \frac{x_p y_p PC}{C + C_0}, \\ \frac{dP}{dt} &= x_p P \left(\frac{y_p C}{C + C_0} - 1\right), \end{aligned} \quad (18)$$

where  $R$ ,  $C$ , and  $P$  are the population densities of the resource, consumer, and predator species, respectively. The system has seven parameters:  $K, x_c, y_c, x_p, y_p, R_0, C_0 > 0$ . Figure 3(b) presents an example of recovering the dynamics of the chaotic food-chain system for  $L_s = 2000$  and  $S_r = 0.85$ . The target output time series for each dimension should contain 2000 points (around 40 cycles of oscillations), but only randomly selected  $L_s \cdot (1 - S_r) = 300$  points are exposed to the trained transformer. The right side of Fig. 3(b) shows the recovered time series, where the three dynamical variables are represented by different colors, the black points indicate observations, and the grey dashed lines are the ground truth. Only a segment of a quarter of the points is displayed. This example demonstrates that, with such a high level of sparsity, directly connecting the observational points will lead to significant errors. Instead, the transformer infers the dynamics by filling the gaps with the correct dynamical behavior. It is worth emphasizing that the testing system has never been exposed to the transformer during the training phase, requiring the neural machine to explore the underlying unknown dynamics from sparse observations based on experience learned from other systems. Extensive results with varying values of the parameters  $L_s$  and  $S_r$  for the three testing systems can be found in Appendix E.

### B. Performance of dynamics reconstruction

To characterize the performance of dynamics reconstruction, we use two measures: MSE [Eq. (14)] and prediction stability  $R_s(\text{MSE}_c)$ , the probability that the transformer generates stable predictions, defined as the probability that the MSE is below a predefined stable

threshold  $\text{MSE}_c$ :

$$R_s(\text{MSE}_c) = \frac{1}{n} \sum_{i=1}^n [\text{MSE} < \text{MSE}_c], \quad (19)$$

where  $n$  is the number of iterations and  $[\cdot] = 1$  if the statement inside is true and zero otherwise. Figure 4(a) shows the working of the framework in the testing phase: a well-trained transformer receives inputs from previously unseen systems, with random sequence length  $L_s$  and sparsity  $S_r$ , and is able to reconstruct the dynamics. Some representative time-series segments of the reconstruction and the ground truth are displayed. Figures 4(b) and 4(c) depict the ensemble-averaged reconstruction performance for the chaotic food chain system. As  $L_s$  increases and  $S_r$  decreases, the transformer can gain more information to facilitate reconstructions. When the available data become more sparse, the performance degrades. Overall, for  $S_r < 0.8$  and a recovered sequence length larger than 500 (about 10 cycles of oscillations in the data), satisfactory reconstruction can be achieved.

It is useful to study how noise affects the dynamics reconstruction. We use normally distributed stochastic processes of zero mean and standard deviation  $\sigma$ , which perturbs the observational points  $x$  to  $x + x \cdot \xi$  after normalization. This is multiplicative or demographic noise commonly encountered in ecological systems. Figure 4(d) shows the effects of the noise on the reconstruction performance, where 50 independent runs are used to calculate the average MSE. The results indicate that, for reasonably small noise (e.g.,  $\sigma < 10^{-1}$ ), robust reconstruction with relatively low MSE values can be achieved. We have also studied the effect of additive noise, with results presented in Appendix F.

### C. Prediction of long-term dynamical climate

The results presented so far are for reconstruction of relatively short term dynamics, where the sequence length  $L_s$  is limited to below 3000, corresponding to approximately 60 cycles of dynamical oscillations in the data. Can the long-term dynamical behavior or climate as characterized by, e.g., a chaotic attractor, be faithfully predicted? To address this question, we note that reservoir computing has the demonstrated ability to generate the long-term behavior of chaotic systems [14, 18, 25, 41, 42]. Our solution is then employing reservoir computing to learn the output time series generated by the transformer so as to further process the reconstructed time series. Assume that a number of sparse data segments are available. The corresponding transformer-reconstructed segments are then used as the training data for the reservoir computer for it to find the relationship between the dynamical state at the current step and that in the immediate future. The trained reservoir computer can predict or generate any length of time series of the target system, as exemplified in Fig. 5(a). It

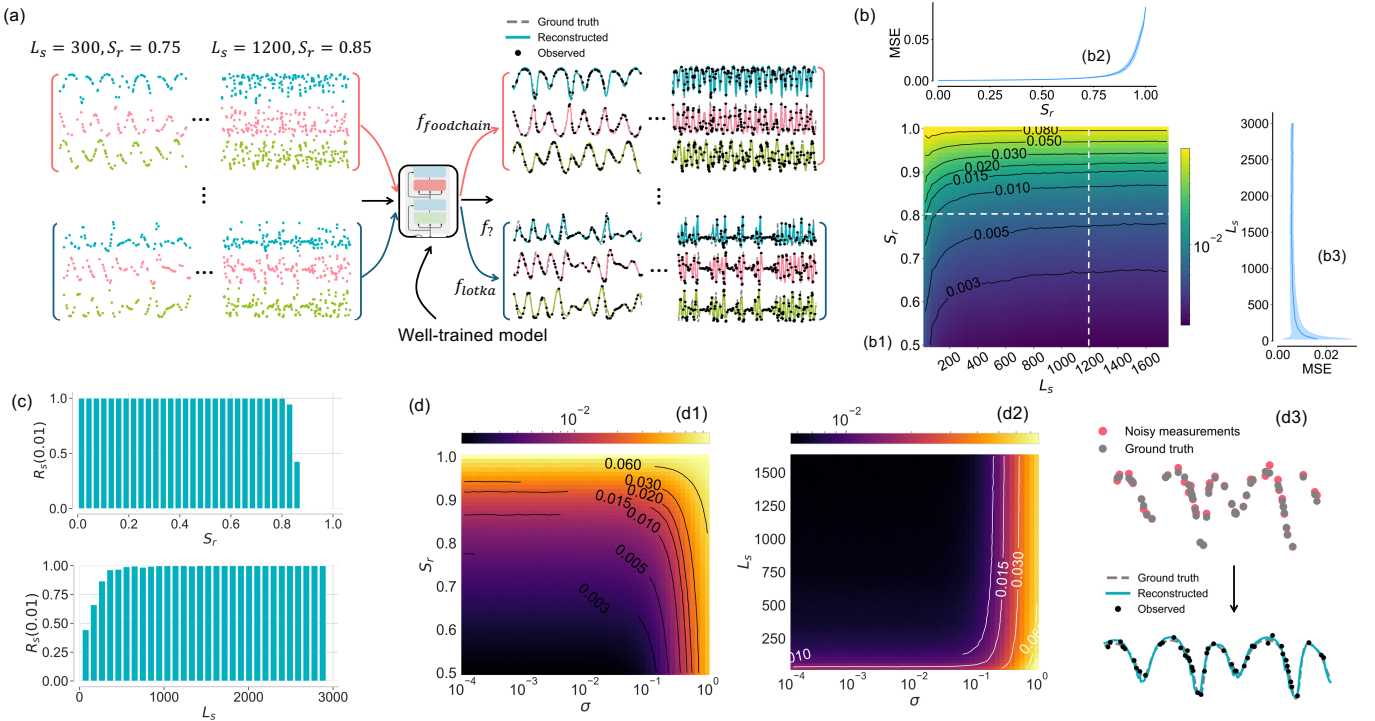


FIG. 4. Performance of dynamics reconstruction. (a) Illustration of reconstruction results for the chaotic food-chain and Lotka-Volterra systems as the testing targets that the transformer has never been exposed to. For each target system, two sets of sparse measurements of different length  $L_s$  and sparsity  $S_r$  are shown. The trained transformer reconstructs the complete time series in each case. (b) Color-coded ensemble-averaged MSE values in the parameter plane  $(L_s, S_r)$  (b1). Examples of testing MSE versus  $S_r$  and  $L_s$  only are shown in (b2) and (b3), respectively. (c) Ensemble-averaged reconstruction stability indicator  $R_s(MSE_c)$  versus  $S_r$  and  $L_s$ , the threshold MSE is  $MSE_c = 0.01$ . (d) Robustness of dynamics reconstruction against noise: ensemble-averaged MSE in the parameter plane  $(\sigma, S_r)$  (d1) and  $(\sigma, L_s)$  (d2), with  $\sigma$  being the noise amplitude. An example of reconstruction under noise of amplitude  $\sigma = 0.1$  is shown in (d3). The values of the performance indicators are the result of averaging over 50 independent statistical realizations.

can be seen that the reservoir-computing generated attractor agrees with the ground truth. More details about reservoir computing, its training and testing can be found in Appendix E.

To evaluate the performance of the reservoir-computing generated long-term dynamics, we use two measures: root MSE (RMSE) and deviation value (DV) characterizing the topological distance between the predicted attractor and the ground truth [41]. Specifically, for a three-dimensional target system, we divide the three-dimensional phase space into a uniform cubic lattice with the cell size  $\Delta = 0.05$  and count the number of trajectory points in each cell, for both the predicted and true attractors in a fixed time interval. The DV measure is defined as

$$DV \equiv \sum_{i=1}^{m_x} \sum_{j=1}^{m_y} \sum_{k=1}^{m_z} \sqrt{(f_{i,j,k} - \hat{f}_{i,j,k})^2}, \quad (20)$$

where  $m_x$ ,  $m_y$ , and  $m_z$  are the total numbers of cells in the  $x$ ,  $y$ , and  $z$  directions, respectively,  $f_{i,j,k}$  and  $\hat{f}_{i,j,k}$  are the frequencies of visit to the cell  $(i, j, k)$  by the predicted and true trajectories, respectively. If the predicted

trajectory leaves the phase space boundary, we count it as if it has landed in the boundary cells where the true trajectory never goes. Figure 5 (b) presents the short- and long-term prediction performance by comparing the reservoir-computing predicted attractors with the ground truth. We calculate the RMSE using a short-term prediction length of 150 (approximately 3 cycles of oscillations), and the DV using a long-term prediction length of 10,000 (corresponding approximately to 200 cycles of oscillations). It can be seen that the reconstructed time series and attractors are close to their respective ground truth when the sparsity parameter  $S_r$  is below 0.8, as indicated by the low RMSE and DV values. The number of available data segments from the target system tends to have a significant effect on the prediction accuracy. Figures 5(c) and 5(d) show the dependence of the DV on two reservoir-computing hyperparameters: the training length  $T_l$  and the reservoir network size  $N_s$ . As the training length and network size increase, DV decreases, indicating improved performance.

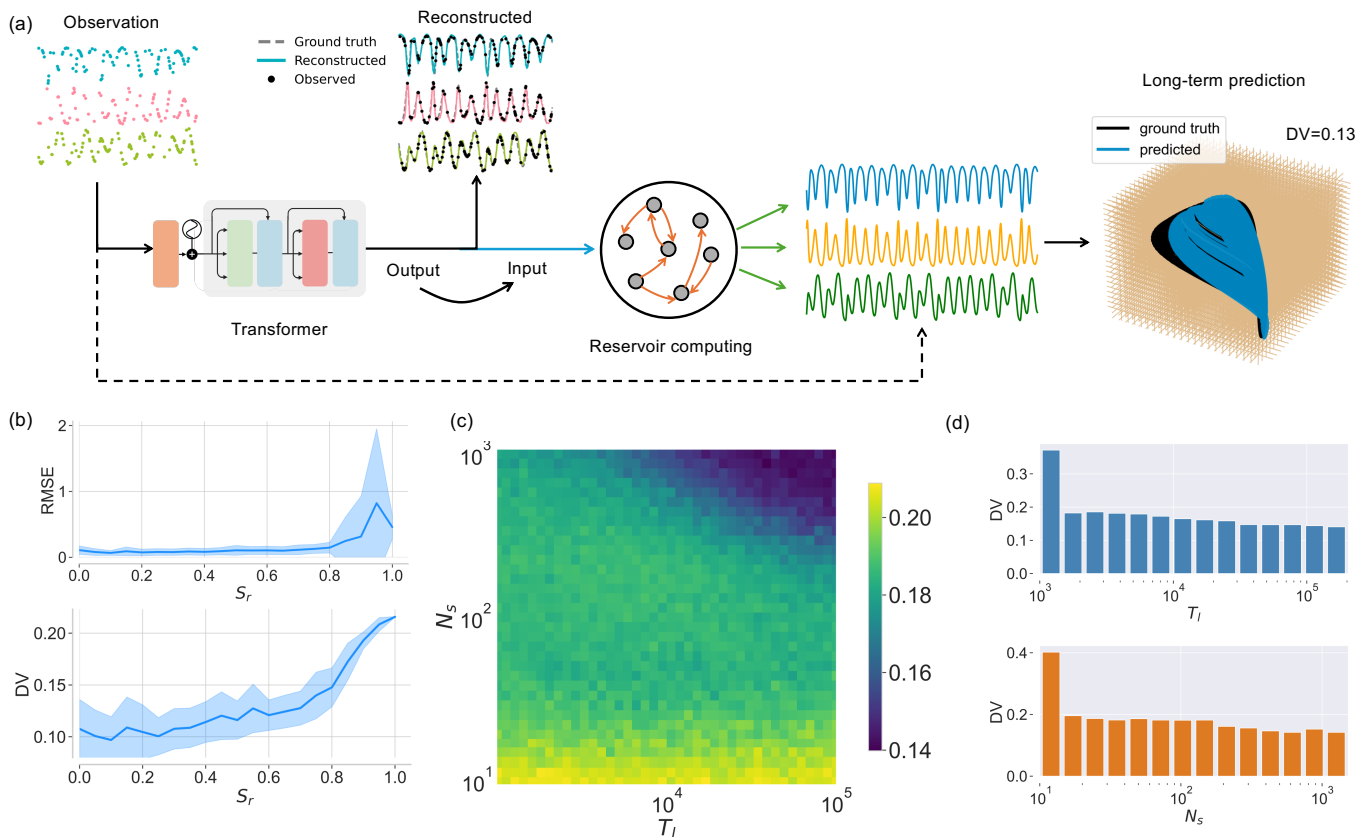


FIG. 5. Reservoir-computing based long-term dynamics prediction. (a) An illustration of hybrid transformer/reservoir-computing framework. The time series reconstructed by the transformer is used to train the reservoir computer that generates time series of the target system of arbitrary length, leading to a reconstructed attractor that agrees with the ground truth. (b) RMSE and DV versus the sparsity parameter. (c) Color-coded ensemble-averaged DV in the reservoir-computing hyperparameter plane ( $T_l, N_s$ ) for  $S_r = 0.8$ . (d) DV versus training length  $T_l$  for  $N_s = 500$  and versus reservoir network size  $N_s$  for  $T_l = 10^5$ . In all cases, 50 independent realizations are used.

#### IV. DISCUSSION

Exploiting machine learning to understand, predict and control the behaviors of nonlinear dynamical systems have demonstrated remarkable success in solving previously deemed difficult problems [43–45]. However, an essential prerequisite for these machine-learning studies is the availability of training data. Often, extensive and uniformly sampled data of the target system are required for training. In addition, in most previous works, training and testing data are from the same system, with a focus on minimizing the average training errors on the specific system and greedily improving the performance by incorporating all correlations within the data, the so-called iid (independently and identically distributed) assumption. While the iid setting can be effective, unforeseen distribution shifts during testing or deployment can cause the optimization purely based on the average training errors to perform poorly [46]. Several strategies have been proposed to handle nonlinear dynamical systems. One approach trains neural networks using data from the same system under different parameter regimes,

enabling prediction of new dynamical behaviors including critical transitions [18]. Another method uses data from multiple systems to train neural networks in tasks like memorizing and retrieving complex dynamical patterns [42, 47]. However, this latter approach fails when encountering novel systems not present in the training data. Meta-learning has been shown to achieve satisfactory performance with only limited data, but training data from the target systems are still required to fine-tune the network weights [48]. In addition, a quite recent work used well-defined, pre-trained large language models not trained using any chaotic data and showed that these models can predict the short-term and long-term dynamics of chaotic systems [49].

We developed a hybrid machine-learning framework to construct the dynamics of target systems, under two limitations: (1) the available observational data are sparse and (2) no training data from the system are available. This requires that the machine-learning framework already be well trained before deploying to the target system. We address this challenge by training the transformer using synthetic or simulated data from numerous

chaotic systems, completely excluding data from the target system. This allows direct application to the target system without fine-tuning. To ensure the transformer’s effectiveness on previously unseen systems, we implement a “triple-randomness” training regime that varies the training systems, input sequence length, and sparsity level. As a result, the transformer will treat each dataset as a new system, rather than adequately learning the dynamics of any single training system. Because of the synthetic nature of the training systems, a massive dataset for each training system is used. This process continues with data from different chaotic systems with random input sequence length and sparsity until the transformer is well-experienced and able to “perceive” the underlying dynamics from the sparse observations. The end result of this training process is that the transformer gains “knowledge” through its experience by adapting to the diverse synthetic datasets. During the testing or deployment phase, the transformer reconstructs dynamics from sparse data of arbitrary length and sparsity drawn from a completely new dynamical system. When multiple segments of sparse observations are available, we can reconstruct the system’s long-term ‘climate’ through a two-step process. First, the transformer repeatedly reconstructs system dynamics from these data segments. Second, reservoir computing uses these transformer-reconstructed dynamics as training data to generate system evolution over any time duration. This hybrid approach, combining transformer and reservoir computing methods, enables reconstruction of the target system’s long-term dynamics and attractor from sparse data alone. The combination of the transformer and reservoir computing constitutes our hybrid machine-learning framework.

We emphasize the key feature of our hybrid framework: recovering the dynamics from sparse observations of an unseen dynamical system, even when the available data has a high degree of sparsity. We have tested the framework on two benchmark ecosystems and one classical chaotic system. In all cases, with extensive training conducted on synthetic datasets under diverse settings, accurate and robust reconstruction has been achieved. Empirically, the minimum requirements for the transformer to be effective are: the dataset from the target system should have the length of at least 20 average cycles of its natural oscillation and the sparsity degree is less than 80%. For the subsequent reservoir computing learning, at least three segments of the time series data from the transformer are needed for reconstructing the attractor of the target system. We have also addressed issues including the effect of noise and hyperparameter optimization. The key to the success of the hybrid framework lies in *versatile dynamics*: with training based on the dynamical data from a diverse array of synthetic systems, the transformer will gain the ability to reconstruct the dynamics of “never-seen” target systems. We have provided a counter example that, when there are no dynamics in the time series, the framework fails to perform

the reconstruction task (see Appendix G).

Our hybrid transformer/reservoir-computing framework represents a powerful tool for dynamics reconstruction and prediction of long-term behavior in situations where only sparse observations from a newly encountered system are available. In fact, such a situation is expected to arise in different fields. For example, in ecosystems, the available data are often limited and incomplete - the reason that we employed two ecosystems as our testing examples. Possible applications extend to medical and biological systems, particularly in wearable health monitoring where data collection is often interrupted. For instance, smartwatches and fitness trackers regularly experience gaps due to charging, device removal during activities like swimming, or signal interference. Another potential application is predicting critical transitions from sparse and noisy observations, such as detecting when an athlete’s performance metrics indicate approaching overtraining, or when a patient’s vital signs suggest an impending health event. In these cases, our hybrid framework can reconstruct complete time series from incomplete wearable device data, serving as input to parameter-adaptable reservoir computing [18, 25, 50] for anticipating these critical transitions. This approach is particularly valuable for continuous health monitoring where data gaps are inevitable, whether from smart devices being charged, removed, or experiencing connectivity issues.

## ACKNOWLEDGMENT

This work was supported by the Air Force Office of Scientific Research under Grant No. FA9550-21-1-0438 and by the Office of Naval Research under Grant No. N00014-24-1-2548.

## Appendix A: Additional background

For dynamical systems reconstruction, machine-learning methods are basically complex approximators mapping inputs to the outputs, or fit relationships among the variables. Deep learning, in particular, is a purely data-driven method that relies on extensive datasets to discover the input-output relationships. This process inherently causes the model to overfit to a specific domain distributed about the training data. As a result, models trained on one dataset often struggle to adapt to unseen data from new distributions, a phenomenon known as out-of-distribution generalization or distribution (covariate) shift [51]. This limitation is particularly pronounced when learning nonlinear dynamics. The challenge is compounded not only by the nonstationary nature of the dynamics but also by changes in the system parameters, which can cause distribution shifts. More extreme shifts can occur when switching between different systems.

Recent years have witnessed a growth of interest in machine learning methods leading to predictive frameworks to estimate data values using unsupervised or supervised learning, due to their nonlinearity, flexibility, and ability to capture useful information embedded in the observed data. Traditional methods include K-nearest neighbor (KNN) [52], support vector machine (SVM) [53], and MissForest [54], etc., but deep learning models are able to deliver more accurate predictions, which include three major categories: recurrent neural network (RNN)-based, generative models, and self-attention based [55]. RNN-based methods [56], featured by their recurrent neural-network structure, are time-consuming and memory-constrained, making it difficult to capture the long-term dependencies within the time series. In addition, the RNN methods are commonly iterative, which inevitably introduces compounding errors through the process. Generative models include generative adversarial network (GAN) [57], variational autoencoder (VAE) [58], and diffusion models [59]. For example, the GAN-based method GAIN [57] takes a generator and a discriminator to predict the data values, where the former imputes the missing values conditioned on the observed data and outputs a reconstructed complete time series, and the latter determines which values are predicted and which belong to the observed data. Generative models provide an adversarial point of view to improve the performance of the generator, but it may suffer from non-convergence or mode collapse due to the loss formulation, and thus are difficult to train [60]. Self-attention-based methods, e.g., transformer models [34], focus on capturing the long-range dependencies and complex relationships within the time series. They excel at handling multi-dimensional data and at tackling input and output sequences of arbitrary length [61]. However, transformer models require substantial amounts of data for effective training and for avoiding overfitting. For instance, a vision transformer (ViT) usually yields low accuracies on mid-size datasets but attains high accuracies when trained on sufficiently large datasets (e.g., 14M-300M images) [62]. Transformer model is thus preferable when the resources are adequate due to its computational efficiency and scalability. Overall, most previous works focused on predicting unobserved values by assembling observable points in various ways, while marginalizing the underlying dynamics, which can be effective for specialized applications but is difficult to be generalized to complex dynamical systems.

It is worth mentioning the related problem of missing data imputation. Handling missing data can be approached through deletion or imputation. Deletion entails removing all entries with missing values [63]. This method is simple and effective when the missing data rate is low, typically less than 10% or 15%, so the removal procedure does not significantly affect the analysis [64]. However, as the missing rate increases, the deletion method becomes less effective and can lead to biased conclusions [65]. In contrast, imputation replaces missing

data with estimated values using statistical or machine learning techniques [66]. Simple imputation methods, such as replacing missing values with the mean or median of the available values, can be readily implemented and are often used during data preprocessing. However, these methods can produce biased or unrealistic results, especially for high-dimensional datasets. Regression is another common imputation technique, where missing values are predicted using a regression model built from complete observations [67]. While effective, this method requires a large amount of data and does not account for any inherent variability. A more advanced approach is the Bayesian method, which treats missing values as unknown parameters drawn from an appropriate probability distribution [68]. This approach allows for the incorporation of prior knowledge about the data distribution and specifies a probabilistic model that captures the relationship between the observed and missing values.

## Appendix B: Adaptation (training) and deployment (testing) systems

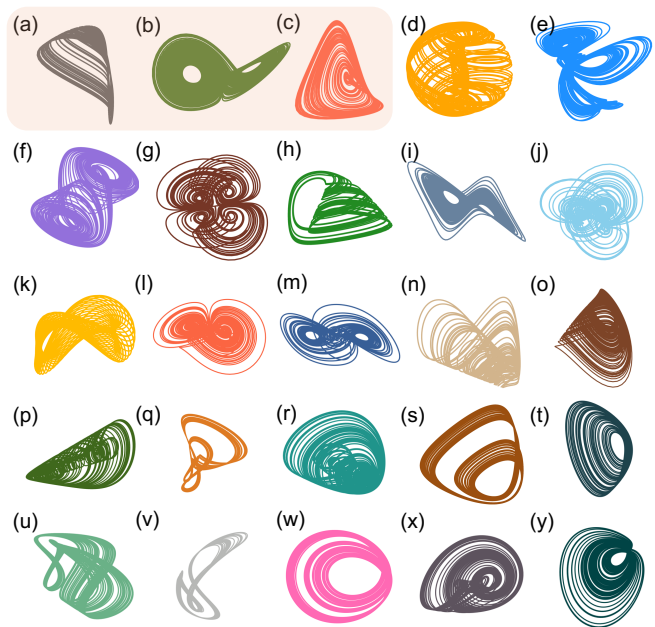


FIG. 6. The chaotic systems for adaptation learning during the training and the target systems for testing. (a-c) Target testing systems: food-chain, Lorenz, and Lota-Volterra systems, respectively. Systems for learning: (d) Aizawa, (e) Bouali, (f) Chua, (g) Four wing, (h) Hastings-Powell, (i) Rikitake, (j) Wang, and (k-y) Spratt systems.

We provide the details of the systems employed during both the adaptation and deployment phases of our hybrid machine-learning framework as in Fig. 6, some of which are collected from [48]. The equations and parameters used to simulate the time series are listed in Tabs. II and III. For the target testing systems, in addition to

the three-species food chain system discussed in detail in the main text, two other systems are tested: the classic chaotic Lorenz system and the Lotka-Volterra system. The Lorenz system is described by

$$\begin{aligned}\frac{dx}{dt} &= \sigma_{lo}(y - x), \\ \frac{dy}{dt} &= x(\rho_{lo} - z) - y, \\ \frac{dz}{dt} &= xy - \beta_{lo}z,\end{aligned}\quad (\text{B1})$$

where  $\sigma_{lo} = 10$ ,  $\rho_{lo} = 2.67$ , and  $\beta_{lo} = 26$  are parameters. The Lotka-Volterra system was originated from the modeling of predator-prey interactions and of certain chemical reactions [38]. For a system of  $N_c$  species with population  $P_i$  ( $i = 1, \dots, N_c$ ) competing for finite resources, the equations are given by

$$\frac{dP_i}{d} = r_i P_i \left(1 - \sum_{j=1}^{N_c} a_{ij} P_j\right), \quad (\text{B2})$$

where  $r_i$  is the growth rate of species  $i$  and  $a_{ij}$  represents characterizes the interaction between species  $j$  and  $i$ . We use the four-species Lotka-Volterra model [38], with the parameter values:

$$r_i = \begin{bmatrix} 1 \\ 0.72 \\ 1.53 \\ 1.27 \end{bmatrix}, \quad a_{ij} = \begin{bmatrix} 1 & 1.09 & 1.52 & 0 \\ 0 & 1 & 0.44 & 1.36 \\ 2.33 & 0 & 1 & 0.47 \\ 1.21 & 0.51 & 0.35 & 1 \end{bmatrix}, \quad (\text{B3})$$

While transformer has the advantage of flexible input data length, the dimension of the input vector needs to be fixed. Since the trained systems are three-dimensional, the target systems should have the same dimension. For the generated four-dimensional Lotka-Volterra time series, we take only data from the first three variables as the target. Since this operation discards the information of the fourth dynamical variable, the reconstruction task becomes even more challenging.

### Appendix C: Reservoir computing

Reservoir computing, a class of recurrent neural networks, is a computational framework designed for efficient training and dynamical systems modeling. It consists of three layers: an input layer, a hidden recurrent layer, and an output layer. Unlike traditional recurrent neural networks where the weights associated all layers are trained, in reservoir computing the input weights and internal recurrent connections remain fixed after random initialization, while only the output weights are adjusted during training through a linear regression. This setting enables efficient training with performance similar to that of the conventional recurrent neural networks [69].

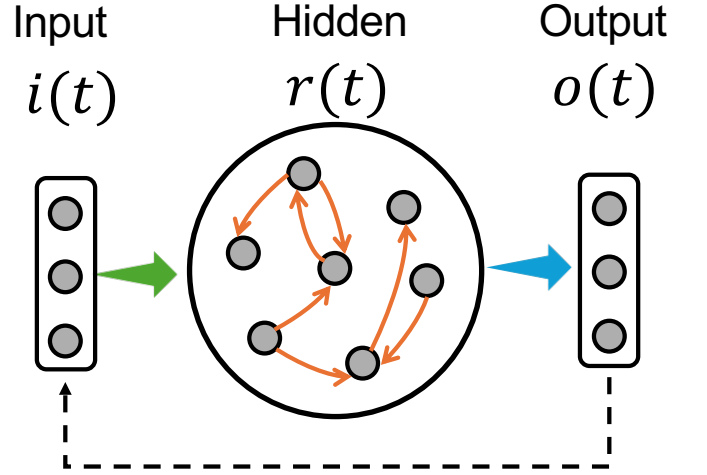


FIG. 7. Basic configuration of reservoir computing.

Figure 7 illustrates the basic structure of reservoir computing, where the input signal  $\mathbf{i}(t)$ , typically a low-dimensional vector, is mapped into the high-dimensional state space in the hidden layer with  $N_s$  nodes by the input matrix  $\mathcal{W}_{\text{in}}$ . Activated by the sequence of reservoir input signals  $[\mathbf{i}(:, 1), \mathbf{i}(:, 2), \dots, \mathbf{i}(:, t)]$ , the hidden layer state  $\mathbf{r}(t)$  is updated step-by-step according to

$$\mathbf{r}(t+1) = (1 - \alpha_r) \cdot \mathbf{r}(t) + \alpha_r \cdot \tanh[\mathcal{A} \cdot \mathbf{r}(t) + \mathcal{W}_{\text{in}} \cdot \mathbf{i}(t)], \quad (\text{C1})$$

where  $\alpha_r$  is the leaking parameter that controls the speed of reservoir memory decays and the nonlinear activation function is of the hyperbolic tangent type. The dimensions of the input signal  $\mathbf{i}(t)$ , hidden state  $\mathbf{r}(t)$ , and output signal  $\mathbf{o}(t)$  are denoted as  $D_i$ ,  $N_s$ , and  $D_o$ , respectively. For three-dimensional chaotic systems, we have  $D_o = D_i = 3$ . The elements of the input matrix  $\mathcal{W}_{\text{in}}$ , which has the dimension of  $N_s * D_i$ , are generated uniformly in the range  $[-\gamma_r, \gamma_r]$  prior to training. The elements of the hidden network  $\mathcal{A}$  of the dimension  $N_s * N_s$ , are Gaussian random numbers generated before training, given the network size  $N_s$ , network link probability  $d_r$ , and spectral radius  $\rho_r$ . The reservoir network size  $N_s$  is typically much larger than input dimension  $D_i$  to ensure that it has sufficient capacity to learn the complex dynamics underlying the input signal. The output matrix  $\mathcal{W}_{\text{out}}$  has the dimension of  $D_o * N_s$ . During the training phase, the reservoir state  $\mathbf{r}(t)$  is updated according to Eq. (C1) and is concatenated into a matrix  $\mathcal{R}$  of the dimension  $N_s * T_l$ , where  $T_l$  is the total training length. With the corresponding input concatenated matrix  $\mathcal{U}$ , the output matrix  $\mathcal{W}_{\text{out}}$  can be obtained by Tikhonov regularization [70] as

$$\mathcal{W}_{\text{out}} = \mathcal{U} \cdot \mathcal{R}^T (\mathcal{R} \cdot \mathcal{R}^T + \beta_r \mathcal{I})^{-1}, \quad (\text{C2})$$

where  $\beta_r$  is the regularization coefficient,  $\mathcal{I}$  is the identity matrix of the dimension  $N_s$ . In the testing phase,

the trained model takes the input  $\mathbf{i}(t)$ , updates the reservoir state  $\mathbf{r}(t)$ , and predicts the output  $\mathbf{o}(t)$  via a linear combination of the reservoir state:

$$\mathbf{o}(\mathbf{t}) = \mathcal{W}_{\text{out}}\mathbf{r}(\mathbf{t}). \quad (\text{C3})$$

As the ground truth data is no longer provided to the reservoir during the testing phase, the output from Eq. (C3) is fed back as the input at the next time step and used to update the hidden states. This process is repeated for any long time until the desired length of dynamical prediction is reached.

## Appendix D: Hyperparameter optimization

Hyperparameter values are essential for machine-learning methods, which can have a significant effect on the performance. We optimize the hyperparameters of transformer and reservoir computing through random search and Bayesian optimization, respectively.

### 1. Transformer hyperparameter optimization

Random search is a simple yet effective method for hyperparameter optimization. Unlike grid search where hyperparameters are tested exhaustively over each possible combination, random search allows sampling hyperparameter values in a larger space. Each time, it randomly selects a combination of the hyperparameters from the search space, evaluates the performance on the validation dataset, and chooses the best performance combination. Due to the large number of hyperparameters the transformer contains, random search is practically effective in terms of the trade-off between the computational cost and performance.

We optimize eleven hyperparameters for transformer through random search, with their values listed in Table I. To gain an intuitive understanding of how these hyperparameter values impact the performance, we test the target systems as they are not used in training and therefore are not used during the hyperparameter optimization process. We compare the prediction performance between the two cases where the hyperparameters are optimized and not. Two chaotic Sprott systems, Sprott0 and Sprott1, are used to find optimal hyperparameters. As transformer is typically “data-greedy,” we not only prepare multiple systems, but for each system, we also provide a sufficient amount of data for training. To demonstrate statistically how much data is required from each training system, we use varying training data length  $D_l$  and evaluate the model performance on target systems. Representative results are shown in Fig. 8. It can be seen that the MSEs are large when  $D_l$  is small, but after reaching a threshold about  $D_l = 10^5$ , the performance improves dramatically. Notably, the sparsity affects the model performance as well: if it is large, in-

creasing  $D_l$  hardly yields any improvement. This is reasonable, as merely increasing the training data for a specific system does not enhance the transformer’s ability to generalize. In fact, it may even hinder the capacity of the model to learn new dynamics due to overfitting on a specific system.

To demonstrate the effectiveness of random search in finding optimal or near-optimal hyperparameter sets, we present the results on the effects of typical hyperparameters on the performance, as depicted in Fig. 9, where all hyperparameters are fixed except one. We train the transformer multiple times to evaluate the effect of varying this hyperparameter on the averaged MSE across trained systems. The results show that in most cases, the hyperparameters determined by random search are indeed optimal or near-optimal for training the transformer.

### 2. Reservoir computing hyperparameter optimization

A key issue of reservoir computing is that its performance often depends sensitively on the hyperparameters. We apply Bayesian optimization from Python (*bayesian-optimization*) to find the optimal values of the following hyperparameters: leakage parameter  $\alpha_r$ , regularization coefficient  $\beta_r$ , input matrix scaling factor  $\gamma_r$ , spectral radius  $\rho_r$ , link probability  $d_r$  determining the network matrix  $\mathcal{A}$ , and the amplitude  $\sigma_r$  of the noise added to the input signal. The optimized hyperparameters are listed in Tab. IV. We evaluate the performance of the reservoir-computing based long-term “climate” or attractor reconstruction with respect to varying the training length  $T_l$  and network size  $N_s$ . Figures 10(a) and 10(b) show the performance versus the two hyperparameters for the Lorenz and Lotka-Volterra systems, respectively. It can be seen that a combination of larger network and longer training length will lead to better reconstruction performance, while increasing the network size for small  $T_l$  will degrade the performance.

## Appendix E: Further demonstration of dynamics reconstruction

### 1. Additional examples of dynamics reconstruction

In the main text, we presented examples of the dynamics reconstruction of the food chain system. To demonstrate that the transformer-based framework performs for varying sparsity  $S_r$  and sequence length  $L_s$ , we present additional examples for the food chain system, as well as the Lorenz and Lotka-Volterra systems, as shown in Figs. 11 and 12, with results comparable to those in the main text: as  $L_s$  increases and  $S_r$  decreases, the performance of the model on target systems continuously improves.

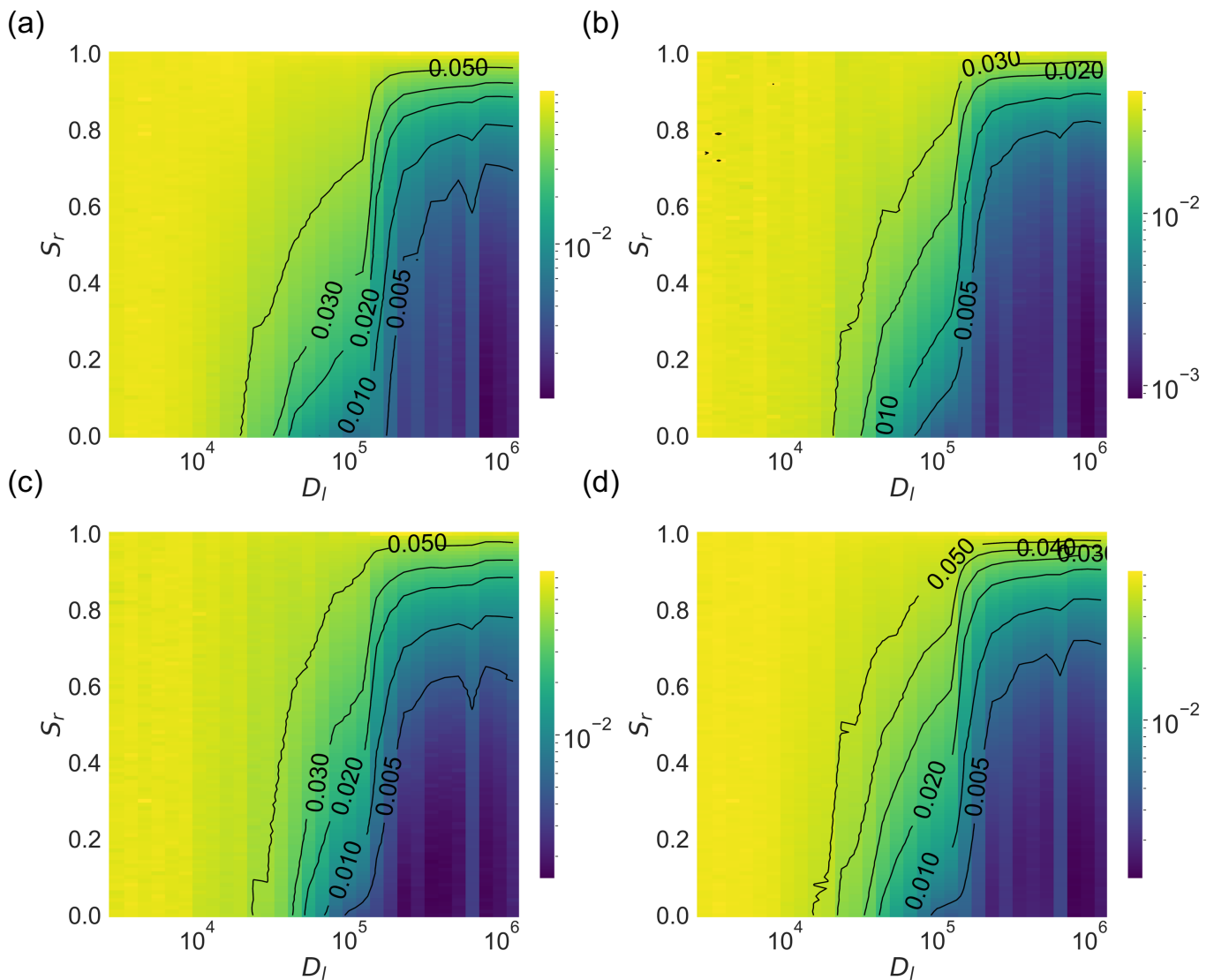


FIG. 8. Effects of the training length  $D_l$  on dynamics recovery performance, for different sparsity  $S_r$ . (a-c) Color-coded ensemble-averaged MSE values in the plane of  $(D_l, S_r)$  for the food-chain, Lorenz, and Lotka-Volterra systems, respectively. (d) Averaged performance over the three systems. Each value of the averaged MSE is obtained using 50 statistical realizations. Increasing the training length can often dramatically improve the prediction performance.

## 2. Performance of system dynamics recovery

In addition to the food chain system in the main text, we further evaluate the performance of the other two target systems. Figure 13 illustrates the reconstruction performance for the Lorenz and Lotka-Volterra systems, as well as the overall performance across all three target systems, as characterized by MSE [see Eq. (14)] and recovery stability [Eq. (19)]. For reconstruction stability analyses,  $L_s$  is fixed at 1,200 (around 25 cycles of oscillations) when varying  $S_r$ , and  $S_r$  is set to 0.8 when varying  $L_s$ . For the Lotka-Volterra system, we set  $S_r$  to 0.75 to ensure reconstruction stability reaching one given sufficient  $L_s$ . These results further demonstrate the ability of the transformer to reconstruct the dynamics of new

systems from sparse observational data.

## 3. Performance of long-term “climate” reconstruction

Reservoir computing utilizes and trains on the reconstructed time series from the transformer and is able to generate arbitrarily long time series with the same statistical properties as those of the original system. Here we present results from long-term reconstruction of the Lorenz and Lotka-Volterra systems, where the time series reconstructed from the transformer are for  $S_r = 0.8$  and 0.75, respectively. Figures 14(a) and 14(b) show segments of the ground truth for the Lorenz and Lotka-

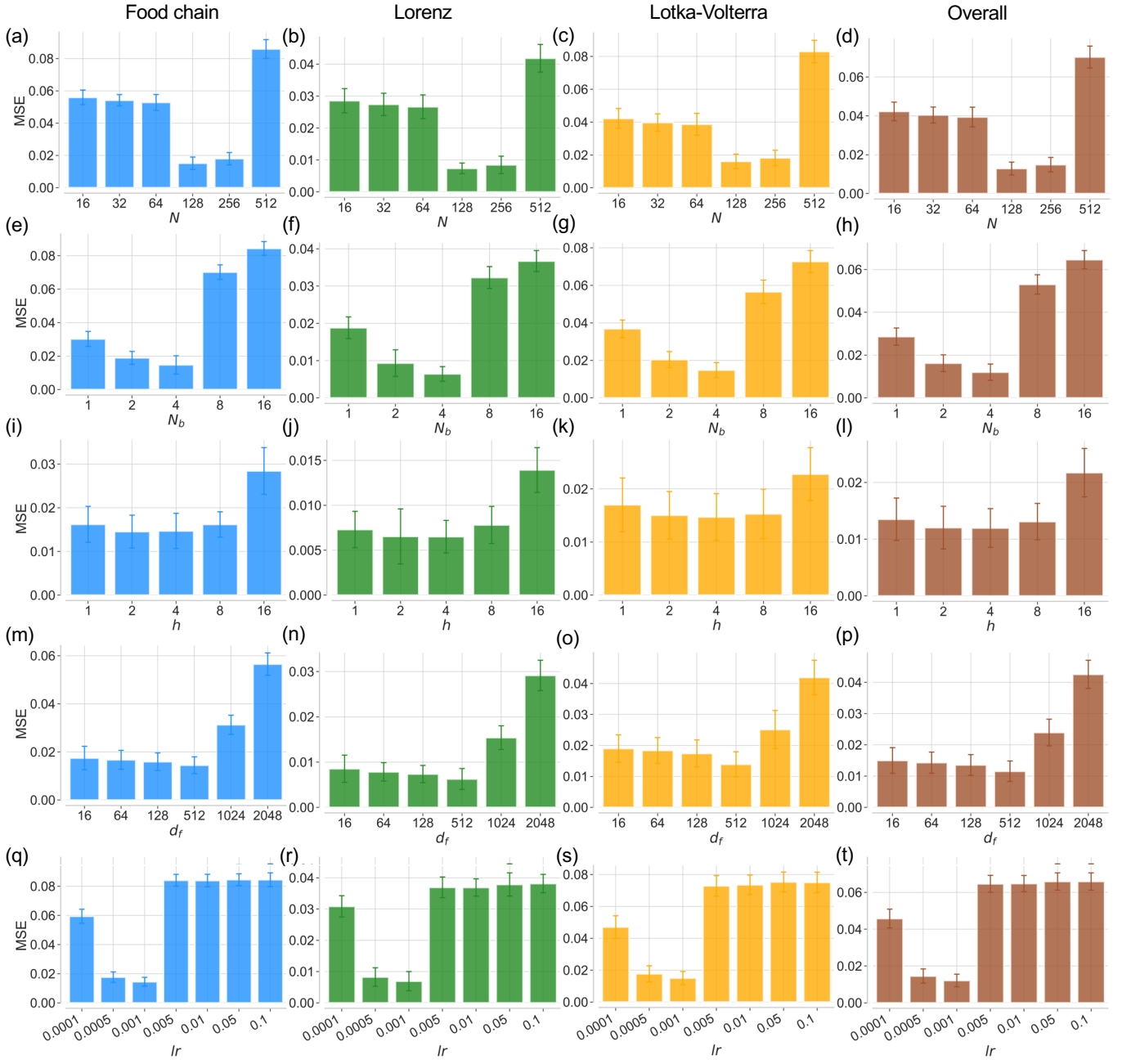


FIG. 9. Effects of representative hyperparameters on performance. Columns 1-4 are the results for the food chain, Lorenz, Lotka-Volterra systems, and the averaged performance of these systems, respectively. Rows 1-5 present the performance with respect to the following hyperparameters: input embedding dimension  $N$ , number  $N_b$  of transformer blocks, transformer heads  $h$ , feedforward neurons  $d_f$ , and learning rate  $lr$ , respectively. To reduce the statistical fluctuations, 50 transformer models are trained to obtain the averaged MSE.

Volterra systems, respectively. Figures 14(c) and 14(d) show the time series generated from reservoir computing for the respective systems. The reconstructed (predicted) and ground truth chaotic attractors of the two systems are depicted in Figs. 14(e) and 14(f), respectively. It can be seen that the reservoir computer can capture the “climate” through the transformer output, providing indirect confirmation that the transformer has

successfully reconstructed the dynamics. Figures 14(g) and 14(h) show the DV versus varying  $S_r$ . In general, as the observations become more sparse, the attractor reconstruction performance as measured by DV gradually degrades. For  $S_r > 0.8$ , the performance deteriorates rapidly.

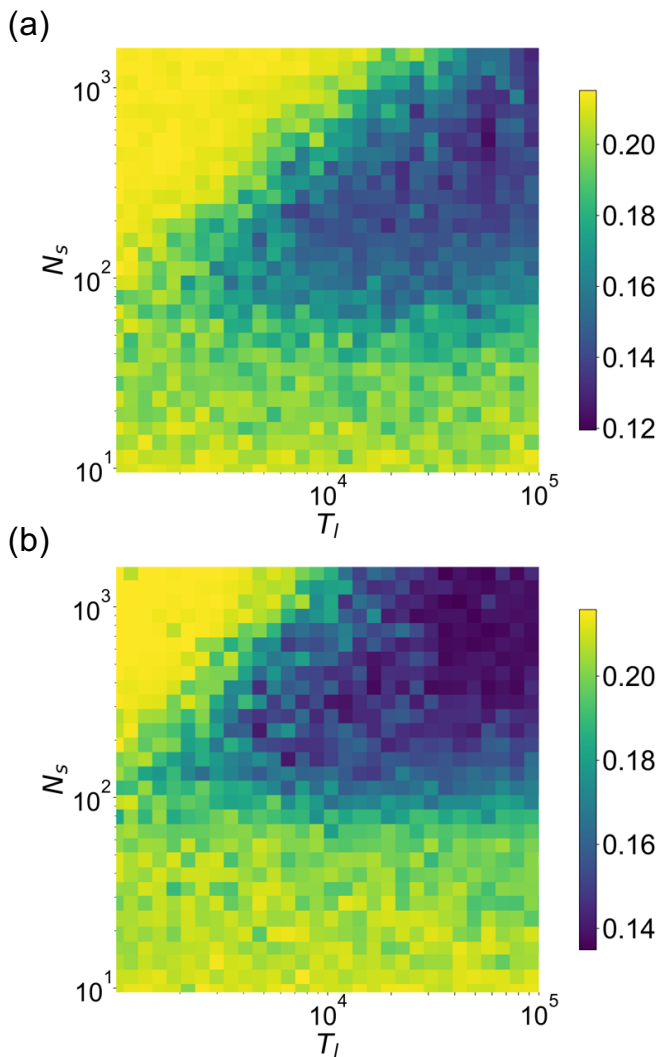


FIG. 10. Effects of reservoir-computing training length and network size on performance. (a,b) Ensemble-averaged MSE obtained from 50 realizations versus changes in the training length  $T_l$  and network size  $N_s$  for the chaotic Lorenz and Lotka-Volterra systems, respectively. Appropriate parameter ranges lead to satisfactory performance.

### Appendix F: Robustness test

We present the results of robustness test against multiplicative and additive noise, for the three target systems, as shown in Figs. 15 and 16. It can be seen that the transformer based dynamics reconstruction framework is robust against multiplicative and additive noise of amplitude below  $10^{-1}$  and  $10^{-1.5}$ , respectively. The sequence length is  $L_s = 1200$  (around 25 cycles of oscillations) for varying  $S_r$  and noise level  $\sigma$ , while  $S_r = 0.8$  for varying  $L_s$ .

### Appendix G: A counter example

For testing, three target systems are presented as examples of reconstructing the system dynamics, assuming that the transformer has never been exposed to these dynamics. This indicates that the transformer trained using data from a large number of synthetic dynamical systems already possesses the ability to find the dynamics behind the sparse data from the target system. To verify that this is indeed the case, we study two scenarios for comparison: (1) the transformer has such a “dynamics-adaptable” ability and (2) it does not have the ability. For the first scenario, we use stochastic signals for testing. Specifically, we generate uniformly distributed noise independently for the three dimensions. A Gaussian filter with the standard deviation  $\sigma_g = 12$  of the Gaussian kernel is applied to smooth the generated noisy data. The resulting stochastic signals are normalized and collected as the testing dataset, as shown in Fig. 17(a). We then take a well-trained transformer adapted for other chaotic systems and test it with the stochastic signal, as shown in Fig. 17(b). For comparison, performance with the food-chain system is shown in Fig. 17(c). For the same sparsity  $S_r$  and sequence length  $L_s$ , the transformer successfully reconstruct the dynamics of the food chain system but completely fails to reconstruct the stochastic signal. The general conclusion is that, the sparse data presented to the transformer need to be associated with some deterministic, nonlinear dynamical process to achieve successful reconstruction.

We further study the performance of the transformer using the stochastic signals and the dynamical systems, as shown Fig. 18. It can be seen that, regardless of the values of  $S_r$  and  $L_s$ , the performance on the target dynamical systems consistently surpasses that on stochastic signals. A performance comparison for  $S_r = 0.5$  is shown in Fig. 18(f). Even with this low sparsity, the transformer is unable to reconstruct the stochastic signal.

### Appendix H: Reconstructing dynamics of diverse chaotic systems

In the main text, we have used 28 chaotic systems for training the transformer and three specific systems for testing. Altogether, 31 chaotic systems have been used. Here we demonstrate that the transformer can also reconstruct arbitrary systems. In particular, each time we choose several systems as the targets for testing, which are excluded from the list of training systems. The remaining chaotic systems are used for training. After training, sparse data from the chosen target system are presented to the transformer for reconstruction. Repeating this process, each and every system in the list of 31 systems can be tested as the target. Representative reconstruction results are shown in Fig. 19, where four systems are chosen as the targets each time. For most systems, the transformer demonstrates can faith-

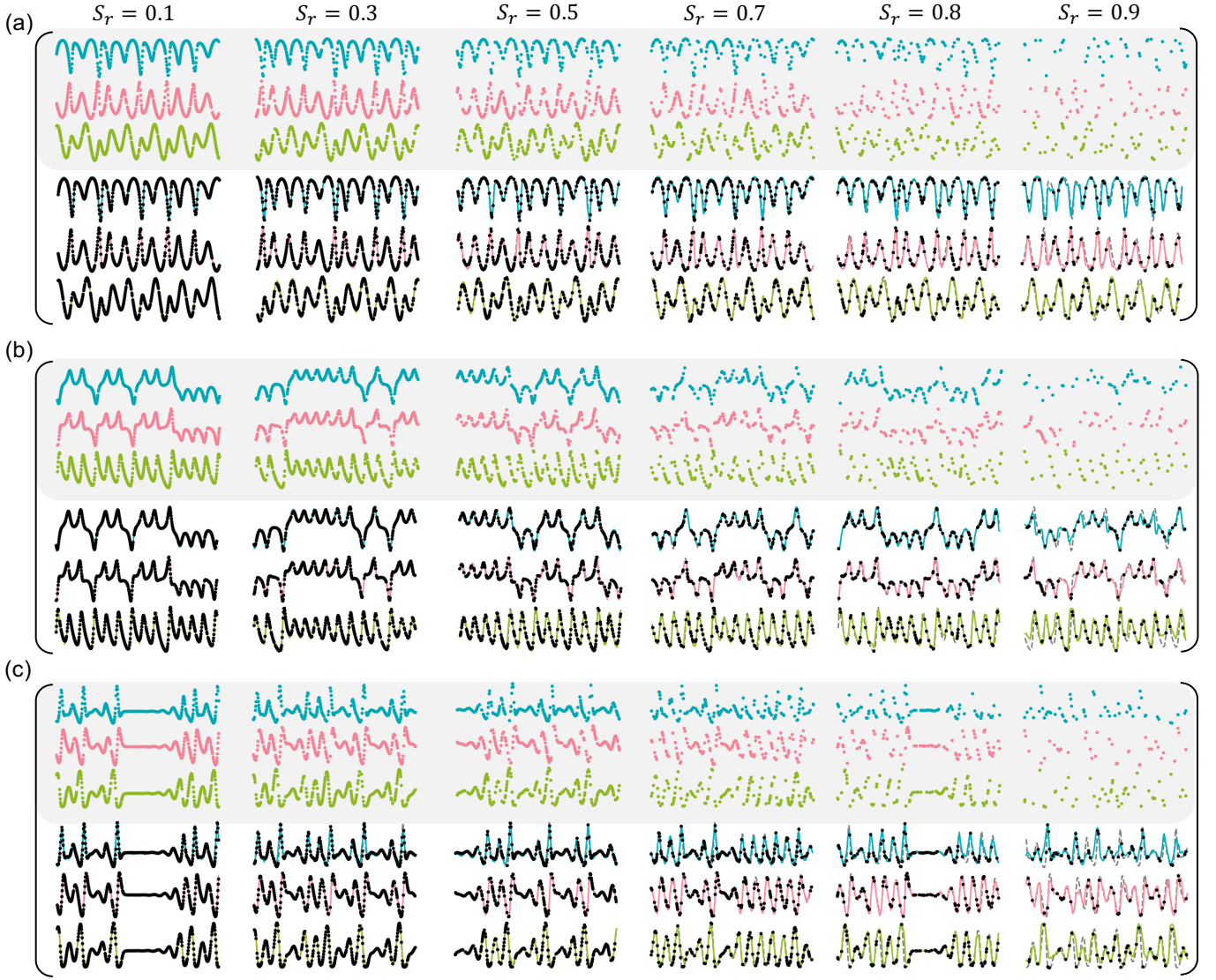


FIG. 11. Additional examples of dynamics reconstruction by transformer for different levels of data sparsity. (a-c) Reconstructed time series for the food chain, Lorenz, and Lotka-Volterra systems, respectively, where the shaded areas represent observable points and unshaded areas show the corresponding reconstruction results. The sequence length is fixed at  $L_s = 1200$  (around 25 cycles of oscillations), but only the first 500 data points are displayed for clarity of presentation.

fully reconstruct the target dynamics for  $S_r = 0.8$  and  $L_s = 1200$ . However, for certain target systems, there is reduced performance. For instance, the construction of the third dimension of the chaotic Rössler system is unsatisfactory, in spite of the excellent reconstruction of the first and second dimensions, as shown in Fig. 19(h). The reason is that the third dynamical variable of the Rössler system exhibits a kind of impulsive behavior. Figure 20 shows the performance of dynamics reconstruction of the 28 different chaotic systems in terms of MSE (a) and reconstruction stability  $R_s(\cdot)$  (b) for  $S_r = 0.8$ . The overall MSE is low the reconstruction is highly stable across all the 28 systems, demonstrating the power and generalizability of the transformer based reconstruction framework.

### Appendix I: Reconstructing dynamics with long short-term memory

Long short-term memory (LSTM) is a type of recurrent neural networks designed to capture the long-term dependencies in sequential data [71]. LSTM has demonstrated remarkable success in time series forecasting, natural language processing, and other tasks, due to its unique cell structure comprising input, forget, and output gates, which regulate the flow of information through the network. The relevant information is retained over extended time steps in LSTM networks, helping them capture temporal dependencies. The basic structure of LSTM is shown in Fig.21(a).

We investigate whether LSTM can be an appropriate

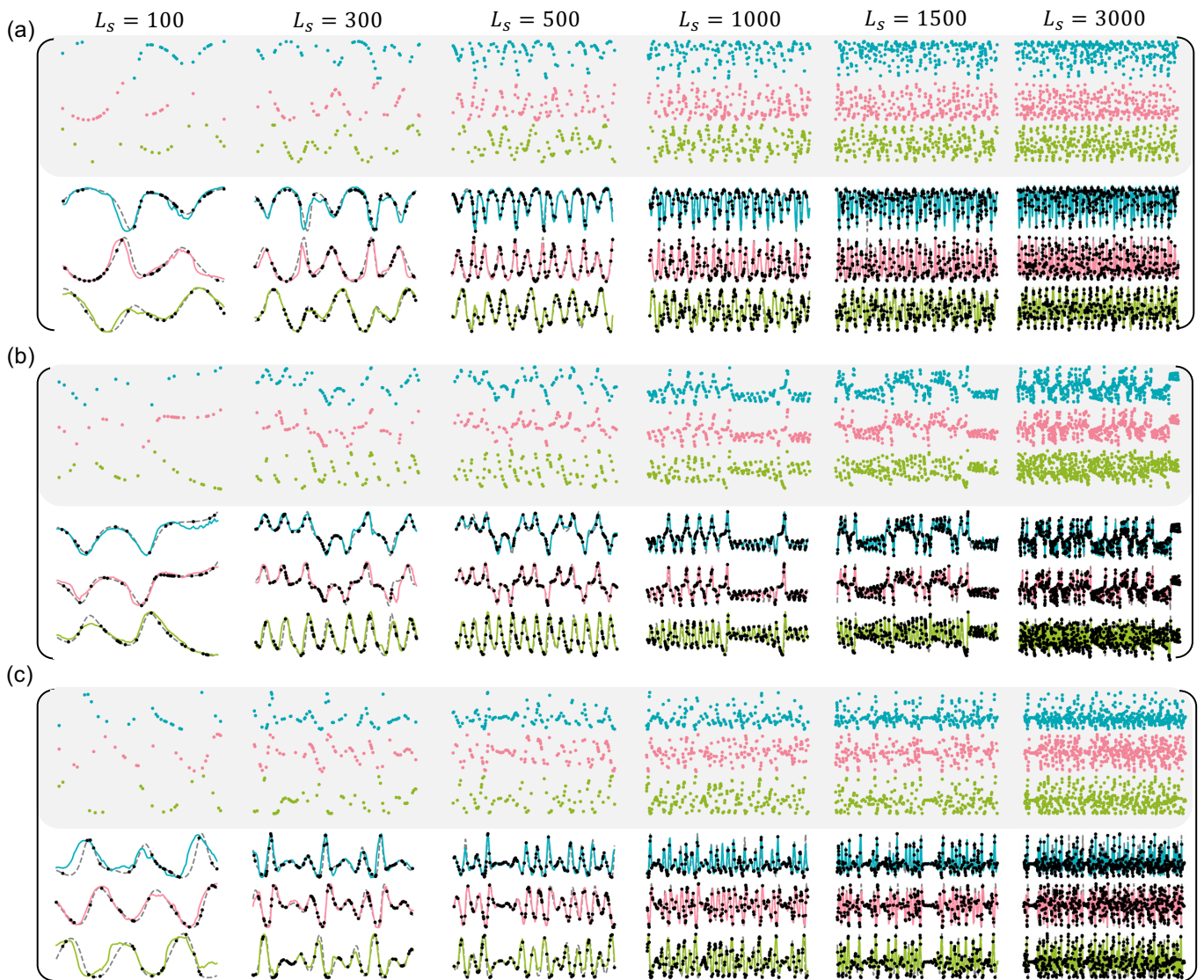


FIG. 12. Additional examples of dynamics reconstruction with respect to varying input sequence length  $L_s$ . (a-c) Reconstructed time series for the food chain, Lorenz, and Lotka-Volterra systems, respectively, where the shaded areas represent the observable points and unshaded areas show the corresponding reconstruction. The sparsity value is fixed at  $S_r = 0.8$ .

substitute for the transformer for dynamics reconstruction from sparse data. To ensure a fair comparison, we keep the hyperparameters as consistent as possible. For example, the hidden network size is set to 512, and the number of layers is set to 4. We train both the LSTM and transformer using the same setup for each training instance, with randomly chosen sequence lengths  $L_s$  and sparsity  $S_r$ , using a batch size of 16 and 50 epochs. The training loss versus the epoch is depicted in Fig. 21(b), indicating that, after the training, the two machine-learning frameworks exhibit similar performance on these training systems. However, for testing, the transformer yields much lower MSE values, as shown in Figs. 21(c) and 21(d). These results suggest that, for dynamics reconstruction from sparse data of unseen dynamical systems, transformer is more effective than traditional re-

current neural networks.

TABLE II. Chaotic systems

Systems	Equations	Parameters
Aizawa	$\begin{aligned}\dot{x} &= (z - b)x - dy \\ \dot{y} &= dx + (z - b)y \\ \dot{z} &= c + az - z^3/3 - (x^2 + y^2)(1 + e^z) + fzx^3\end{aligned}$	$\begin{aligned}a &= 0.95, b = 0.7, c = 0.6 \\ d &= 3.5, e = 0.25, f = 0.1\end{aligned}$
Bouali	$\begin{aligned}\dot{x} &= x(a - y) + \alpha z \\ \dot{y} &= -y(b - x^2) \\ \dot{z} &= -x(c - sz) - \beta z\end{aligned}$	$\begin{aligned}\alpha &= 0.3, \beta = 0.05 \\ a &= 4, b = 1, c = 1.5, s = 1\end{aligned}$
Chua	$\begin{aligned}\dot{x} &= \alpha(y - x - ht) \\ \dot{y} &= \gamma(x - y + z) \\ \dot{z} &= -\beta y\end{aligned}$	$\begin{aligned}\alpha &= 15.6, \gamma = 1, \beta = 28 \\ \mu_0 &= -1.143, \mu_1 = -0.714 \\ ht &= \mu_1 x + 0.5(\mu_0 - \mu_1)( x + 1  -  x - 1 )\end{aligned}$
Dadras	$\begin{aligned}\dot{x} &= y - ax + byz \\ \dot{y} &= cy - xz + z \\ \dot{z} &= dxy - ez\end{aligned}$	$\begin{aligned}a &= 3, b = 2.7 \\ c &= 1.7, d = 2, e = 9\end{aligned}$
Four wing	$\begin{aligned}\dot{x} &= ax + yz \\ \dot{y} &= bx + cy - xz \\ \dot{z} &= -z - xy\end{aligned}$	$a = 0.2, b = 0.01, c = -0.4$
Hastings-Powell	$\begin{aligned}\dot{V} &= V(1 - V) - a_1VH/(b_1V + 1) \\ \dot{H} &= a_1VH/(b_1V + 1) - a_2HP/(b_2H + 1) - d_1H \\ \dot{P} &= a_2HP/(b_2H + 1) - d_2P\end{aligned}$	$\begin{aligned}a_1 &= 5, a_2 = 0.1 \\ b_1 &= 3, b_2 = 2 \\ d_1 &= 0.4, d_2 = 0.01\end{aligned}$
Rikitake	$\begin{aligned}\dot{x} &= -\mu x + zy \\ \dot{y} &= -\mu y + x(z - a) \\ \dot{z} &= 1 - xy\end{aligned}$	$\mu = 2, a = 5$
Rossler	$\begin{aligned}\dot{x} &= -(y + z) \\ \dot{y} &= x + ay \\ \dot{z} &= b + z(x - c)\end{aligned}$	$a = 0.2, b = 0.2, c = 5.7$
Wang	$\begin{aligned}\dot{x} &= x - yz \\ \dot{y} &= x - y + xz \\ \dot{z} &= -az + xy\end{aligned}$	$a = 3$

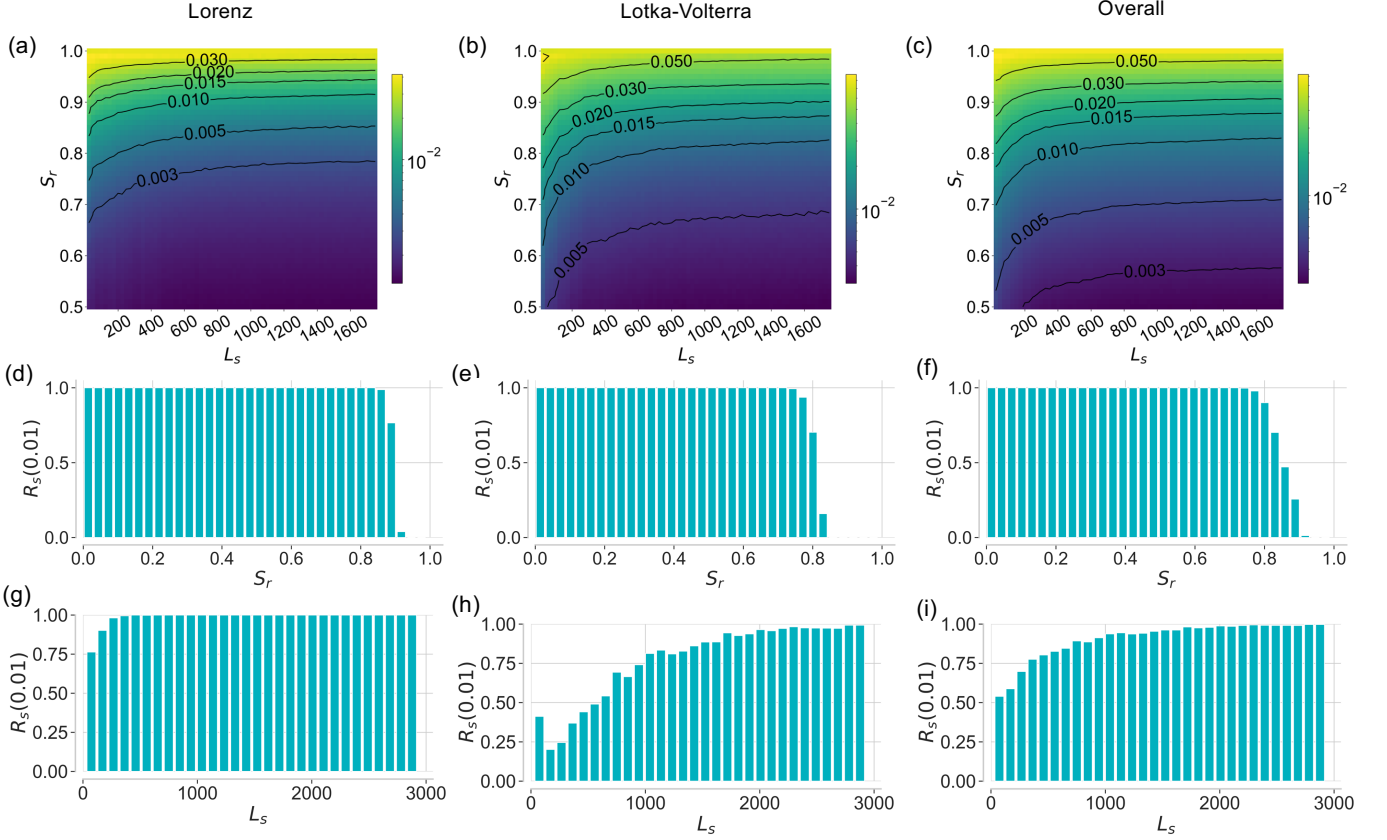


FIG. 13. Dynamics reconstruction performance. The three columns are the results for the Lorenz, and Lotka-Volterra systems, and the averaged performance over the three target systems, respectively. The three rows from top to down present the color-coded averaged MSE in the parameter plane ( $L_s, S_r$ ), the recovery stability  $R_s$  versus  $S_r$  and  $L_s$  for MSE threshold 0.01, respectively. Reconstruction stability and averaged MSE are calculated from 400,000 data points (corresponding to around 8,000 cycles of oscillations) in each case.

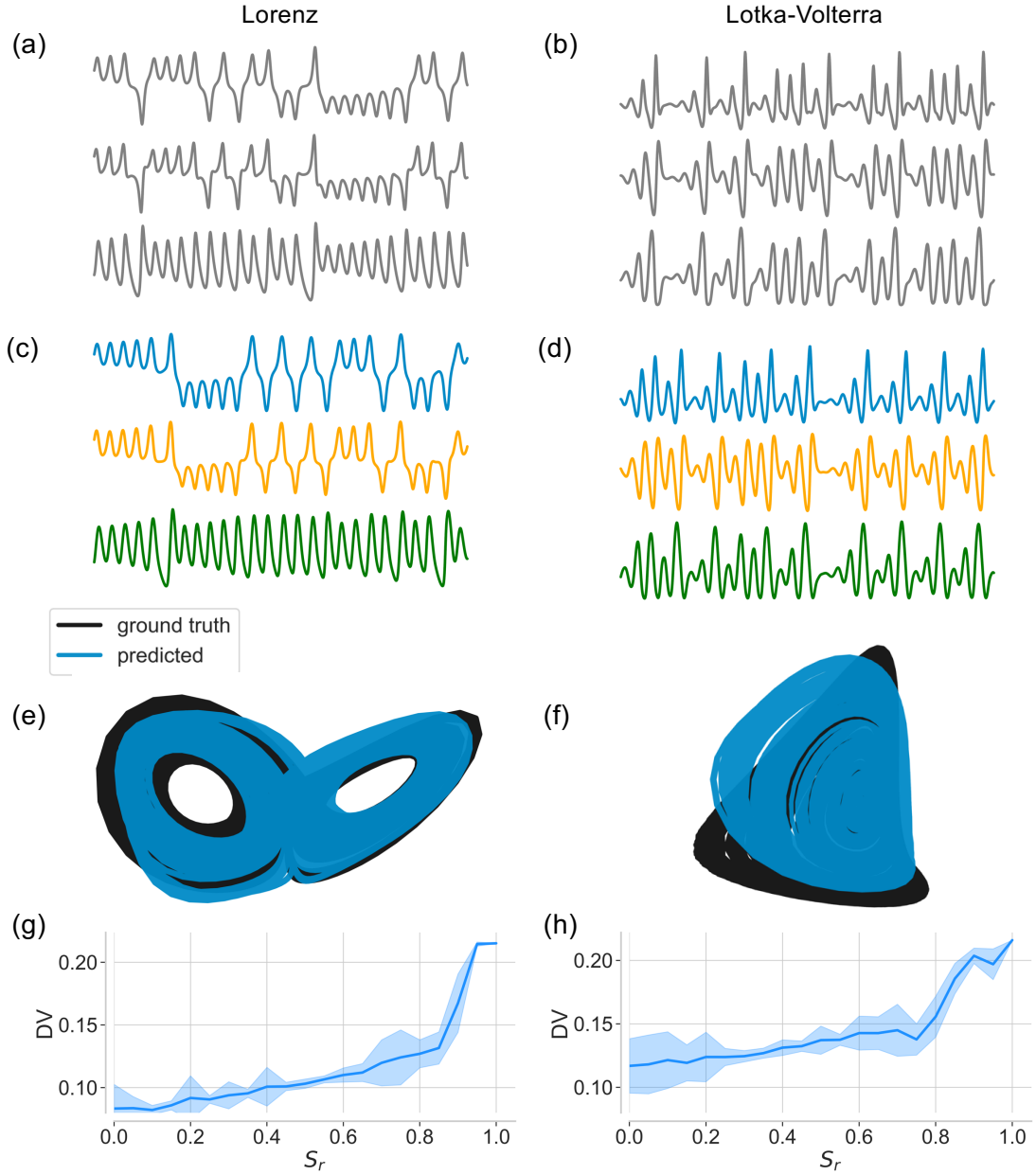


FIG. 14. Attractor reconstruction by reservoir computing. The first and second columns are for the Lorenz and Lotka-Volterra systems, respectively. (a,b) Segments of ground truth time series, (c,d) short-term predictions by reservoir computing, (e,f) reconstructed long-term attractors as compared with the true attractors, and (g, f) ensemble-averaged DV versus sparsity  $S_r$ , obtained from 50 independent realizations.

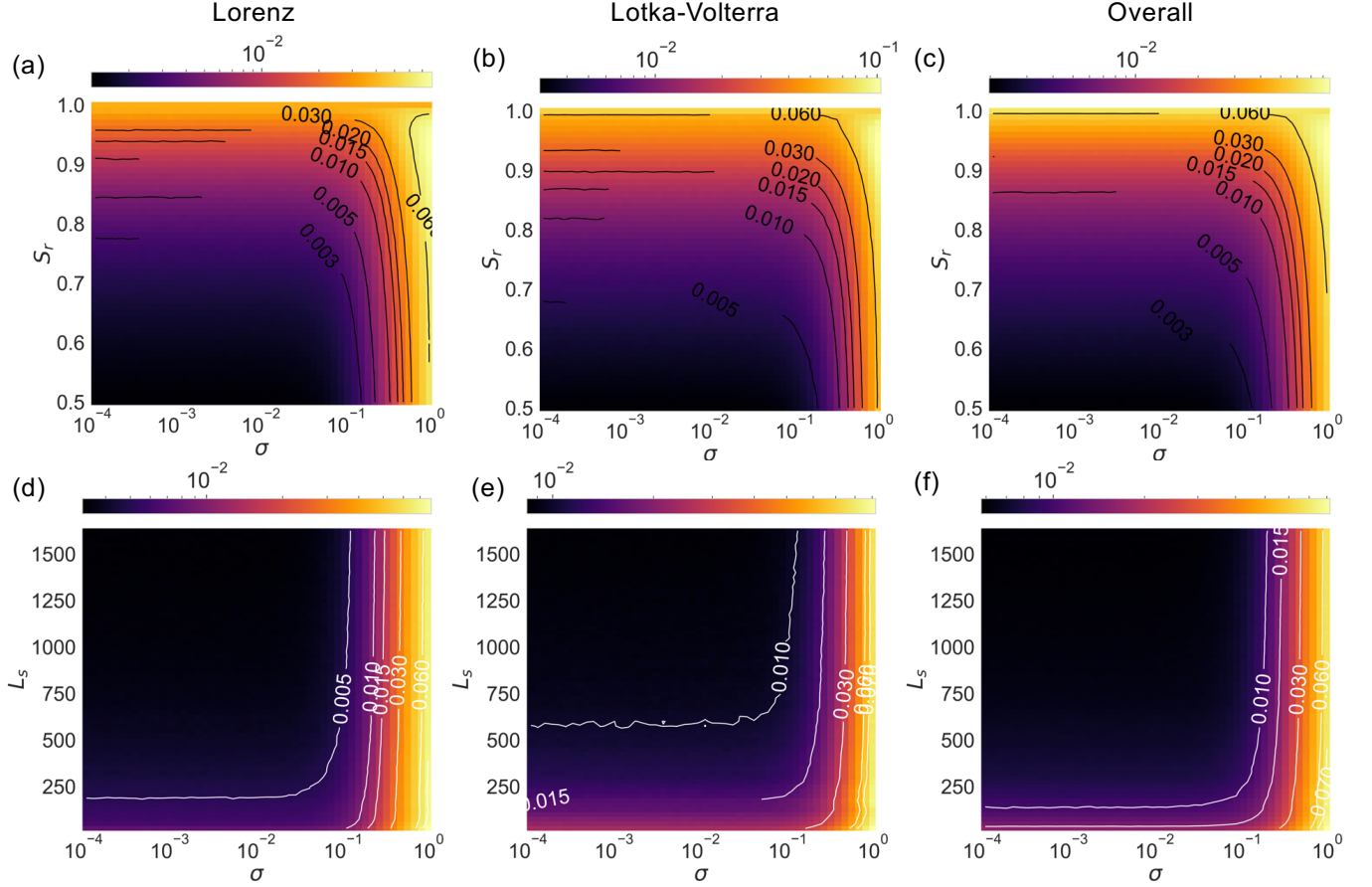


FIG. 15. Robustness against multiplicative noise. Three columns represent results for the Lorenz, and Lotka-Volterra systems, and the averaged performance over the three target systems, respectively. The two rows show ensemble-averaged, color-coded MSE from 50 independent realizations, over the parameter planes  $(\sigma, S_r)$  and  $(\sigma, L_s)$ , respectively. The results indicate that the transformer-based dynamics-reconstruction framework is robust against multiplicative noise.

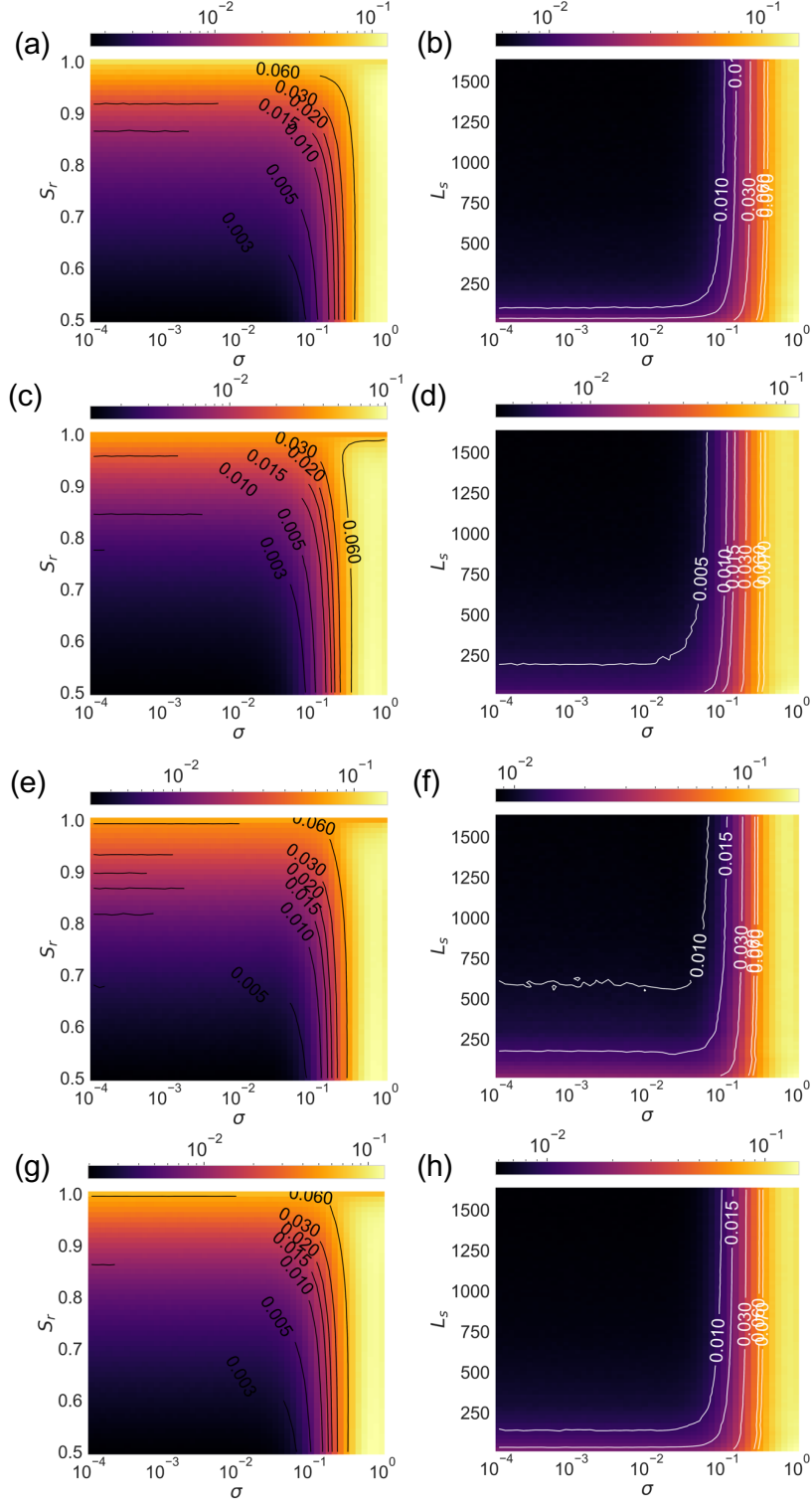


FIG. 16. Robustness against additive noise. The four rows represent results for the food chain, Lorenz, Lotka-Volterra systems, and the overall performance, respectively. The two columns show ensemble-averaged, color-coded MSE from 50 independent realizations, over the parameter planes  $(\sigma, S_r)$  and  $(\sigma, L_s)$ , respectively. The transformer-based dynamics reconstruction framework is robust against additive noise.

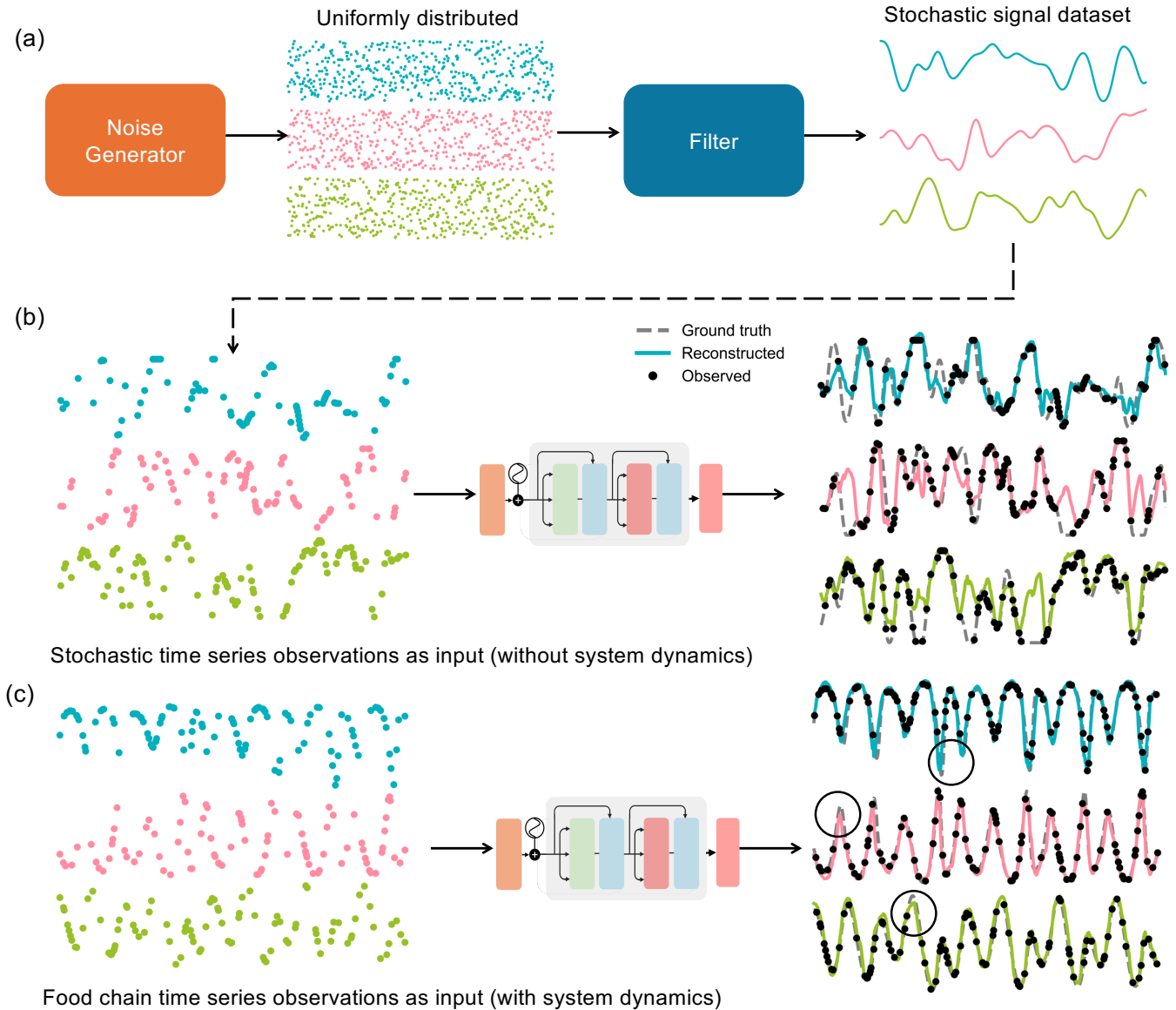


FIG. 17. Illustration of stochastic signal recovery. (a) Generation of the stochastic signal dataset. (b,c) Examples of reconstructing time series without and with underlying system dynamics by using a well-trained transformer for  $L_s = 1200$  (around 25 cycles of oscillations) and  $S_r = 0.8$ .

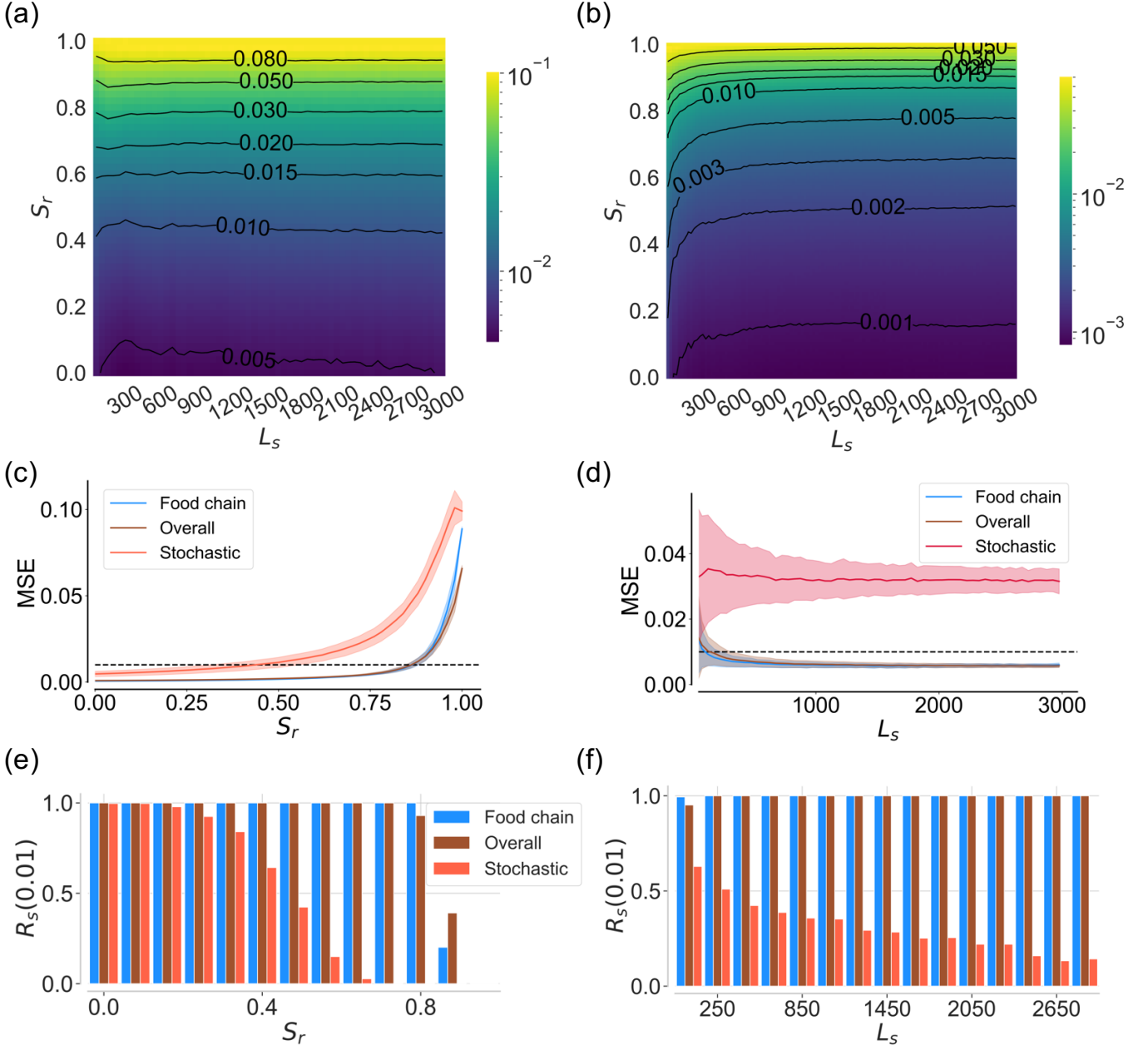


FIG. 18. Performance of transformer on stochastic signals and target systems. (a,b) Ensemble-averaged color-coded MSE in the parameter plane  $(L_s, S_r)$  for the stochastic and target dynamical systems, respectively, (c) MSE versus  $S_r$  for  $L_s = 1200$  (around 25 cycles), (d) MSE versus  $L_s$  for  $S_r = 0.8$ , (e) reconstruction stability  $R_s(\cdot)$  versus  $S_r$  for  $L_s = 1200$ , (f) reconstruction stability  $R_s(\cdot)$  versus  $L_s$  for  $S_r = 0.5$ . The reconstruction stability and the averaged MSE are calculated from 400,000 data points (corresponding to around 8,000 cycles) in each case.

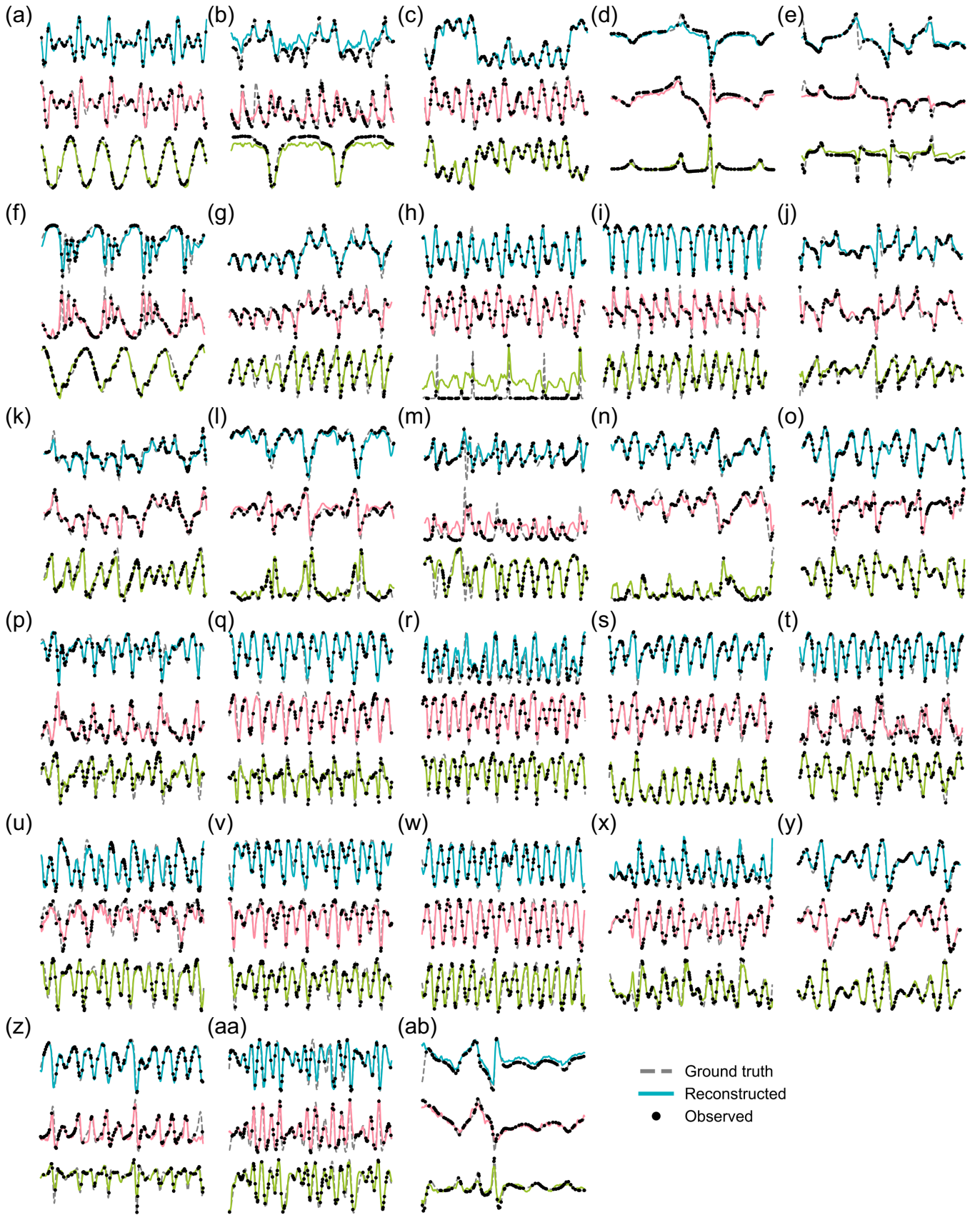


FIG. 19. Dynamics reconstruction of 28 different chaotic systems: (a) Aizawa, (b) Bouali, (c) Chua, (d) Dadras, (e) Four wing, (f) Hastings-Powell, (g) Rikitake, (h) Rossler, (i-aa) Sprott systems. (ab) Wang system, for  $S_r = 0.8$  and  $L_s = 1200$  (around 25 cycles).

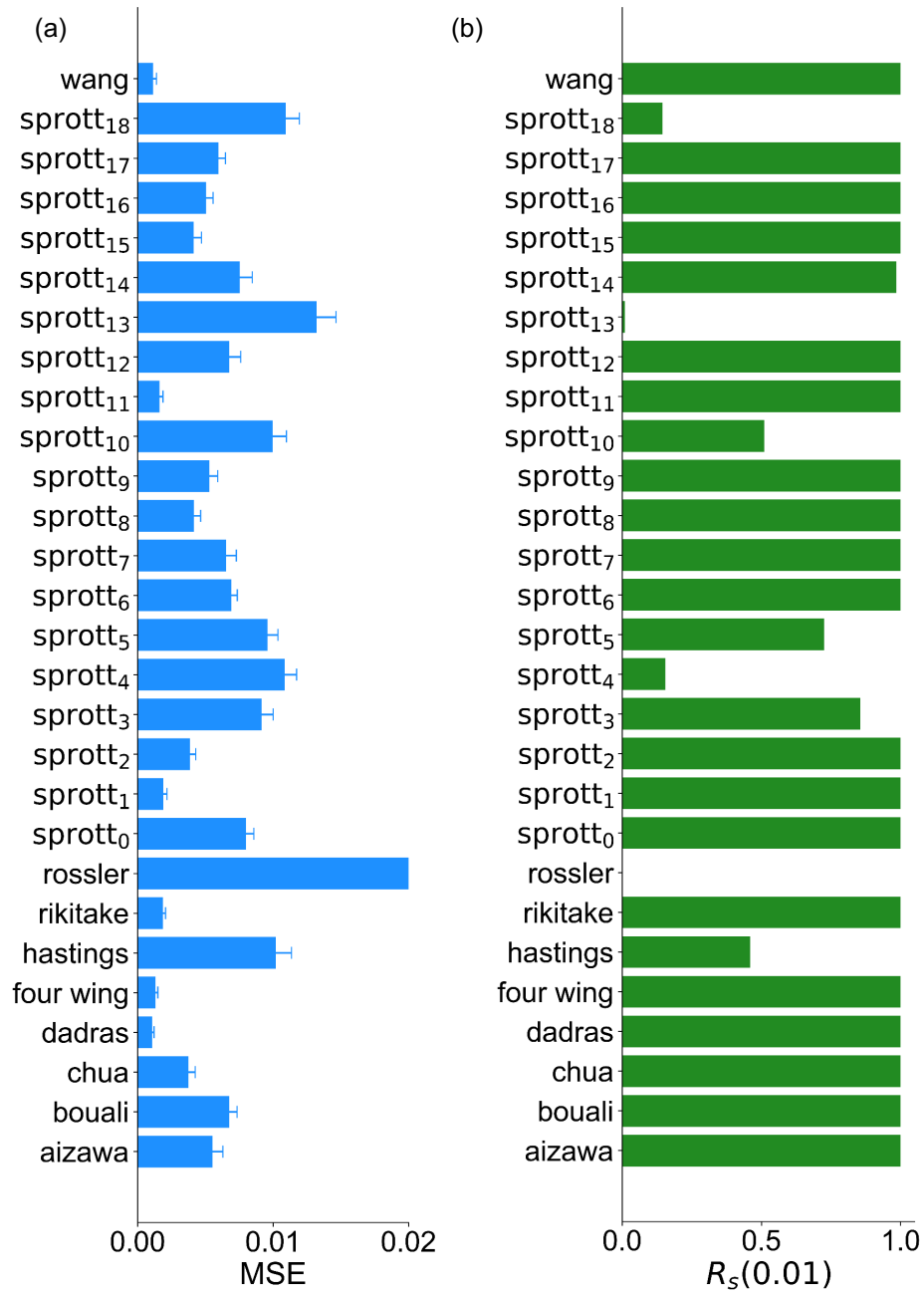


FIG. 20. Performance of dynamics reconstruction on the 28 chaotic systems. (a) Averages MSEs calculated from 400,000 data points (corresponding to about 8,000 cycles of oscillations) in each case. (b) Reconstruction stability  $R_s(\cdot)$  for  $S_r = 0.8$  and  $L_s = 1200$  (about 25 cycles).

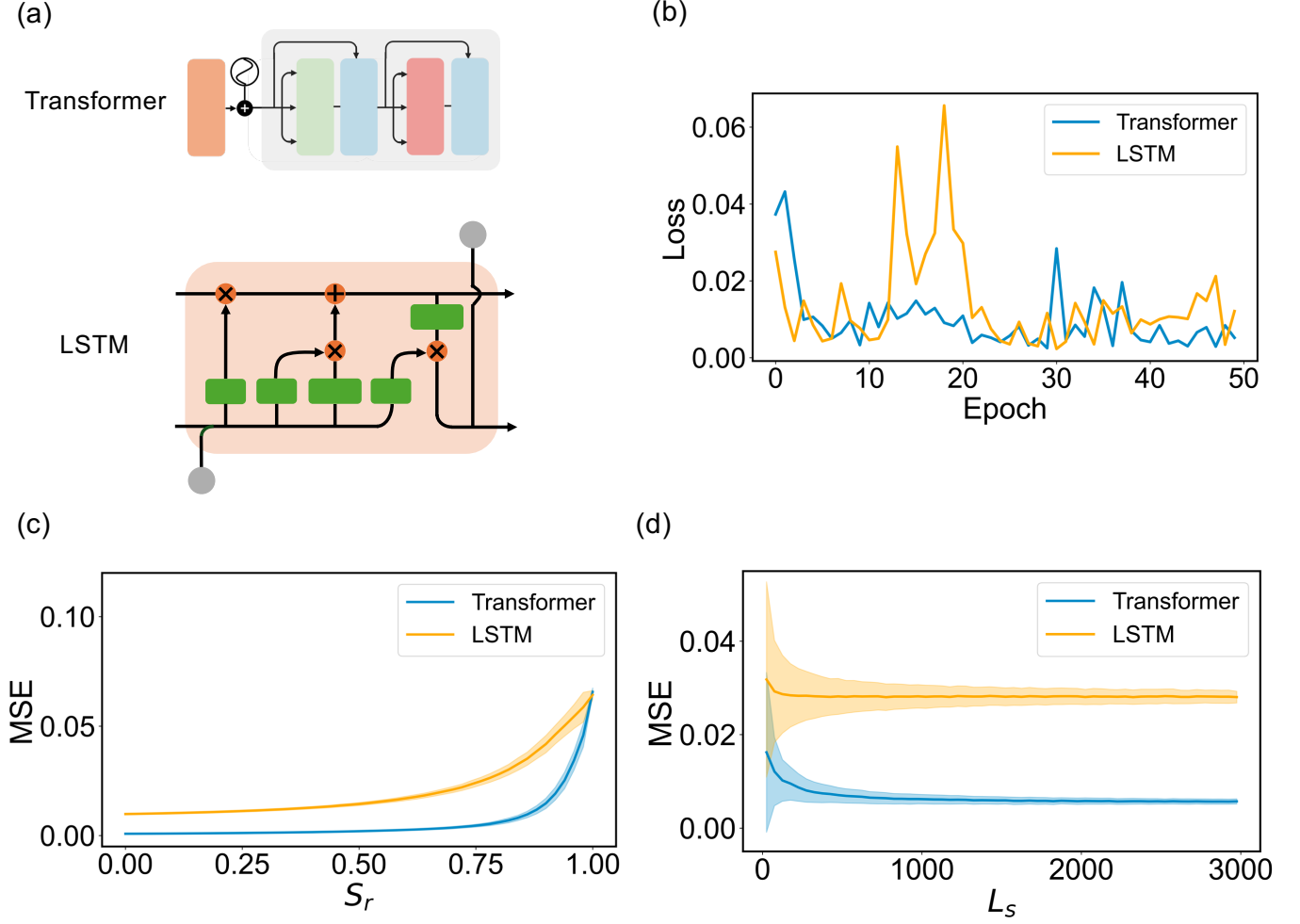


FIG. 21. Comparison of dynamics reconstruction performance between transformer and LSTM. (a) Basic structures of the two machine learning frameworks. (b) Training loss of transformer and LSTM. (c) MSE versus  $S_r$  for transformer and LSTM for  $L_s = 1200$  (around 25 cycles). (d) MSE versus  $L_s$  for  $S_r = 0.8$ . Averaged MSEs are calculated from 400,000 data points (corresponding to around 8,000 cycles of oscillations) in each case, for the food chain, Lorenz, and Lotka-Volterra systems.

TABLE III. Chaotic sprcott systems

Case	Equations
0	$\dot{x} = y, \dot{y} = -x + yz, \dot{z} = 1 - y^2$
1	$\dot{x} = yz, \dot{y} = x - y, \dot{z} = 1 - xy$
2	$\dot{x} = yz, \dot{y} = x - y, \dot{z} = 1 - x^2$
3	$\dot{x} = -y, \dot{y} = x + z, \dot{z} = xz + 3y^2$
4	$\dot{x} = yz, \dot{y} = x^2 - y, \dot{z} = 1 - 4x$
5	$\dot{x} = y + z, \dot{y} = -x + 0.5y, \dot{z} = x^2 - z$
6	$\dot{x} = 0.4x + z, \dot{z} = xz - y, \dot{y} = -x + y$
7	$\dot{x} = -y + z^2, \dot{y} = x + 0.5y, \dot{z} = xz$
8	$\dot{x} = -0.2y, \dot{y} = x + z, \dot{z} = x + y^2 - z$
9	$\dot{x} = 2z, \dot{y} = -2y + z, \dot{z} = -x + y + y^2$
10	$\dot{x} = xy - z, \dot{y} = x - y, \dot{z} = x + 0.3z$
11	$\dot{x} = y + 3.9z, \dot{y} = 0.9x^2 - y, \dot{z} = 1 - x$
12	$\dot{x} = -z, \dot{y} = -x^2 - y, \dot{z} = 1.7 + 1.7x + y$
13	$\dot{x} = -2y, \dot{y} = x + z^2, \dot{z} = 1 + y - 2z$
14	$\dot{x} = y, \dot{y} = x - z, \dot{z} = x + xz + 2.7y$
15	$\dot{x} = 2.7y + z, \dot{y} = -x + y^2, \dot{z} = x + y$
16	$\dot{x} = -z, \dot{y} = x - y, \dot{z} = 3.1x + y^2 + 0.5z$
17	$\dot{x} = 0.9 - y, \dot{y} = 0.4 + z, \dot{z} = xy - z$
18	$\dot{x} = -x - 4y, \dot{y} = x + z^2, \dot{z} = 1 + x$

TABLE IV. Optimal hyperparameter values of reservoir computing for target systems

System	$\alpha_r$	$\beta_r$	$\gamma_r$	$\rho_r$	$d_r$	$\sigma_r$
Food chain	0.36	$10^{-1.25}$	1.16	1.29	0.41	$10^{-4.70}$
Lorenz	0.30	$10^{-5.15}$	1.82	1.30	0.68	$10^{-2.04}$
Lotka-Volterra	0.29	$10^{-6.62}$	0.19	1.72	0.02	$10^{-2.73}$

- 
- [1] W.-X. Wang, R. Yang, Y.-C. Lai, V. Kovanis, and C. Grebogi, Predicting catastrophes in nonlinear dynamical systems by compressive sensing, *Phys. Rev. Lett.* **106**, 154101 (2011).
- [2] Y.-C. Lai, Finding nonlinear system equations and complex network structures from data: A sparse optimization approach, *Chaos* **31**, 082101 (2021).
- [3] N. D. Haynes, M. C. Soriano, D. P. Rosin, I. Fischer, and D. J. Gauthier, Reservoir computing with a single time-delay autonomous Boolean node, *Phys. Rev. E* **91**, 020801 (2015).
- [4] L. Larger, A. Baylón-Fuentes, R. Martinenghi, V. S. Udaltsov, Y. K. Chembo, and M. Jacquot, High-speed photonic reservoir computing using a time-delay-based architecture: Million words per second classification, *Phys. Rev. X* **7**, 011015 (2017).
- [5] J. Pathak, Z. Lu, B. Hunt, M. Girvan, and E. Ott, Using machine learning to replicate chaotic attractors and calculate Lyapunov exponents from data, *Chaos* **27**, 121102 (2017).
- [6] Z. Lu, J. Pathak, B. Hunt, M. Girvan, R. Brockett, and E. Ott, Reservoir observers: Model-free inference of unmeasured variables in chaotic systems, *Chaos* **27**, 041102 (2017).
- [7] J. Pathak, B. Hunt, M. Girvan, Z. Lu, and E. Ott, Model-free prediction of large spatiotemporally chaotic systems from data: A reservoir computing approach, *Phys. Rev. Lett.* **120**, 024102 (2018).
- [8] T. L. Carroll, Using reservoir computers to distinguish chaotic signals, *Phys. Rev. E* **98**, 052209 (2018).
- [9] K. Nakai and Y. Saiki, Machine-learning inference of fluid variables from data using reservoir computing, *Phys. Rev. E* **98**, 023111 (2018).
- [10] Z. S. Roland and U. Parlitz, Observing spatio-temporal dynamics of excitable media using reservoir computing, *Chaos* **28**, 043118 (2018).
- [11] A. Griffith, A. Pomerance, and D. J. Gauthier, Forecasting chaotic systems with very low connectivity reservoir computers, *Chaos* **29**, 123108 (2019).
- [12] J. Jiang and Y.-C. Lai, Model-free prediction of spatiotemporal dynamical systems with recurrent neural networks: Role of network spectral radius, *Phys. Rev. Res.* **1**, 033056 (2019).
- [13] G. Tanaka, T. Yamane, J. B. Héroux, R. Nakane, N. Kanazawa, S. Takeda, H. Numata, D. Nakano, and A. Hirose, Recent advances in physical reservoir computing: A review, *Neu. Net.* **115**, 100 (2019).
- [14] H. Fan, J. Jiang, C. Zhang, X. Wang, and Y.-C. Lai, Long-term prediction of chaotic systems with machine learning, *Phys. Rev. Res.* **2**, 012080 (2020).
- [15] C. Zhang, J. Jiang, S.-X. Qu, and Y.-C. Lai, Predicting phase and sensing phase coherence in chaotic systems with machine learning, *Chaos* **30**, 083114 (2020).
- [16] C. Klos, Y. F. K. Kossio, S. Goedeke, A. Gilra, and R.-M. Memmesheimer, Dynamical learning of dynamics, *Phys. Rev. Lett.* **125**, 088103 (2020).
- [17] P. Chen, R. Liu, K. Aihara, and L. Chen, Autoreservoir computing for multistep ahead prediction based on the spatiotemporal information transformation, *Nat. Commun.* **11**, 4568 (2020).
- [18] L.-W. Kong, H.-W. Fan, C. Grebogi, and Y.-C. Lai, Machine learning prediction of critical transition and system collapse, *Phys. Rev. Res.* **3**, 013090 (2021).
- [19] D. Patel, D. Canaday, M. Girvan, A. Pomerance, and E. Ott, Using machine learning to predict statistical properties of non-stationary dynamical processes: System climate, regime transitions, and the effect of stochasticity, *Chaos* **31**, 033149 (2021).
- [20] J. Z. Kim, Z. Lu, E. Nozari, G. J. Pappas, and D. S. Bassett, Teaching recurrent neural networks to infer global temporal structure from local examples, *Nat. Machine Intell.* **3**, 316 (2021).
- [21] H. Fan, L.-W. Kong, Y.-C. Lai, and X. Wang, Anticipating synchronization with machine learning, *Phys. Rev. Res.* **3**, 023237 (2021).
- [22] L.-W. Kong, H.-W. Fan, C. Grebogi, and Y.-C. Lai, Emergence of transient chaos and intermittency in machine learning, *J. Phys. Complex.* **2**, 035014 (2021).
- [23] E. Bollt, On explaining the surprising success of reservoir computing forecaster of chaos? The universal machine learning dynamical system with contrast to VAR and DMD, *Chaos* **31**, 013108 (2021).
- [24] D. J. Gauthier, E. Bollt, A. Griffith, and W. A. Barbosa, Next generation reservoir computing, *Nat. Commun.* **12**, 1 (2021).
- [25] L.-W. Kong, Y. Weng, B. Glaz, M. Haile, and Y.-C. Lai, Reservoir computing as digital twins for nonlinear dynamical systems, *Chaos* **33**, 033111 (2023).
- [26] Z.-M. Zhai, L.-W. Kong, and Y.-C. Lai, Emergence of a resonance in machine learning, *Phys. Rev. Res.* **5**, 033127 (2023).
- [27] M. Yan, C. Huang, P. Bienstman, P. Tino, W. Lin, and J. Sun, Emerging opportunities and challenges for the future of reservoir computing, *Nat. Commun.* **15**, 2056 (2024).
- [28] Z.-M. Zhai, M. Moradi, L.-W. Kong, B. Glaz, M. Haile, and Y.-C. Lai, Model-free tracking control of complex dynamical trajectories with machine learning, *Nat. Commun.* **14**, 5698 (2023).
- [29] Z.-M. Zhai, M. Moradi, L.-W. Kong, and Y.-C. Lai, Detecting weak physical signal from noise: A machine-learning approach with applications to magnetic-anomaly-guided navigation, *Phys. Rev. Appl.* **19**, 034030 (2023).
- [30] Z.-M. Zhai, M. Moradi, B. Glaz, M. Haile, and Y.-C. Lai, Machine-learning parameter tracking with partial state observation, *Phys. Rev. Res.* **6**, 013196 (2024).
- [31] Z. Liu, Y. Wang, S. Vaidya, F. Ruehle, J. Halverson, M. Soljačić, T. Y. Hou, and M. Tegmark, Kan: Kolmogorov-Arnold networks, *arXiv preprint arXiv:2404.19756* (2024).
- [32] M. Moradi, S. Panahi, E. M. Bollt, and Y.-C. Lai, Data-driven model discovery with Kolmogorov-Arnold networks, *arXiv preprint arXiv:2409.15167* (2024).
- [33] K. Yeo, Data-driven reconstruction of nonlinear dynamics from sparse observation, *J. Comput. Phys.* **395**, 671 (2019).
- [34] A. Vaswani, N. Shazeer, N. Parmar, J. Uszkoreit, L. Jones, A. N. Gomez, Ł. Kaiser, and I. Polosukhin, Attention is all you need, *Adv. Neural Inf. Process. Syst.* **30** (2017).
- [35] A. Y. Yıldız, E. Koç, and A. Koç, Multivariate time se-

- ries imputation with transformers, *IEEE Signal Process. Lett.* **29**, 2517 (2022).
- [36] K. McCann and P. Yodzis, Nonlinear dynamics and population disappearances, *Am. Nat.* **144**, 873 (1994).
- [37] E. N. Lorenz, Deterministic nonperiodic flow, *J. Atmos. Sci.* **20**, 130 (1963).
- [38] J. Vano, J. Wildenberg, M. Anderson, J. Noel, and J. Sprott, Chaos in low-dimensional Lotka-Volterra models of competition, *Nonlinearity* **19**, 2391 (2006).
- [39] F. Nogueira, Bayesian Optimization: Open source constrained global optimization tool for Python (2014–).
- [40] J. Bergstra and Y. Bengio, Random search for hyperparameter optimization., *J. Mach. Learn. Res.* **13** (2012).
- [41] Z.-M. Zhai, L.-W. Kong, and Y.-C. Lai, Emergence of a resonance in machine learning, *Phys. Rev. Res.* **5**, 033127 (2023).
- [42] L.-W. Kong, G. A. Brewer, and Y.-C. Lai, Reservoir-computing based associative memory and itinerancy for complex dynamical attractors, *Nat. Commun.* **15**, 4840 (2024).
- [43] Z.-M. Zhai, M. Moradi, L.-W. Kong, B. Glaz, M. Haile, and Y.-C. Lai, Model-free tracking control of complex dynamical trajectories with machine learning, *Nat. Commun.* **14**, 5698 (2023).
- [44] J. Z. Kim and D. S. Bassett, A neural machine code and programming framework for the reservoir computer, *Nat. Mach. Intell.* **5**, 622 (2023).
- [45] Z.-M. Zhai, M. Moradi, B. Glaz, M. Haile, and Y.-C. Lai, Machine-learning parameter tracking with partial state observation, *Phys. Rev. Res.* **6**, 013196 (2024).
- [46] J. Liu, Z. Shen, Y. He, X. Zhang, R. Xu, H. Yu, and P. Cui, Towards out-of-distribution generalization: A survey, *arXiv preprint arXiv:2108.13624* (2021).
- [47] Y. Du, H. Luo, J. Guo, J. Xiao, Y. Yu, and X. Wang, Multi-functional reservoir computing, *arXiv preprint arXiv:2409.16719* (2024).
- [48] Z.-M. Zhai, B. Glaz, M. Haile, and Y.-C. Lai, Learning to learn ecosystems from limited data - a meta-learning approach, *arXiv preprint arXiv:2410.07368* (2024).
- [49] Y. Zhang and W. Gilpin, Zero-shot forecasting of chaotic systems, *arXiv preprint arXiv:2409.15771* (2024).
- [50] S. Panahi and Y.-C. Lai, Adaptable reservoir computing: A paradigm for model-free data-driven prediction of critical transitions in nonlinear dynamical systems, *Chaos* **34**, 051501 (2024).
- [51] R. Yu and R. Wang, Learning dynamical systems from data: An introduction to physics-guided deep learning, *Proc. Natl. Acad. Sci. U.S.A.* **121**, e2311808121 (2024).
- [52] G. E. Batista, M. C. Monard, *et al.*, A study of k-nearest neighbour as an imputation method., *His* **87**, 48 (2002).
- [53] K. Pelckmans, J. De Brabanter, J. A. Suykens, and B. De Moor, Handling missing values in support vector machine classifiers, *Neural Netw.* **18**, 684 (2005).
- [54] D. J. Stekhoven and P. Bühlmann, Missforest-non-parametric missing value imputation for mixed-type data, *Bioinformatics* **28**, 112 (2012).
- [55] W. Du, D. Côté, and Y. Liu, Saits: Self-attention-based imputation for time series, *Expert Syst. Appl.* **219**, 119619 (2023).
- [56] Z. Che, S. Purushotham, K. Cho, D. Sontag, and Y. Liu, Recurrent neural networks for multivariate time series with missing values, *Sci. Rep.* **8**, 6085 (2018).
- [57] J. Yoon, J. Jordon, and M. Schaar, Gain: Missing data imputation using generative adversarial nets, in *Proc. Int. Conf. Mach. Learn.* (PMLR, 2018) pp. 5689–5698.
- [58] S. Ramchandran, G. Tikhonov, K. Kujanpää, M. Koskinen, and H. Lähdesmäki, Longitudinal variational autoencoder, in *Proc. Int. Conf. Artif. Intell. Stat.* (PMLR, 2021) pp. 3898–3906.
- [59] X. Wang, H. Zhang, P. Wang, Y. Zhang, B. Wang, Z. Zhou, and Y. Wang, An observed value consistent diffusion model for imputing missing values in multivariate time series, in *Proc. 29th ACM SIGKDD Conf. Knowl. Discov. Data Min.* (2023) pp. 2409–2418.
- [60] T. Salimans, I. Goodfellow, W. Zaremba, V. Cheung, A. Radford, and X. Chen, Improved techniques for training gans, *Adv. Neural Inf. Process. Syst.* **29** (2016).
- [61] J. Liu, S. Pasumarthi, B. Duffy, E. Gong, K. Datta, and G. Zaharchuk, One model to synthesize them all: Multi-contrast multi-scale transformer for missing data imputation, *IEEE Trans. Med. Imaging.* **42**, 2577 (2023).
- [62] A. DOSOVITSKIY, An image is worth 16x16 words: Transformers for image recognition at scale, *arXiv preprint arXiv:2010.11929* (2020).
- [63] T. Emmanuel, T. Maupong, D. Mpoeleng, T. Semong, B. Mphago, and O. Tabona, A survey on missing data in machine learning, *J. Big Data.* **8**, 1 (2021).
- [64] K. Strike, K. El Emam, and N. Madhavji, Software cost estimation with incomplete data, *IEEE Trans. Softw. Eng.* **27**, 890 (2001).
- [65] E. Acuna and C. Rodriguez, The treatment of missing values and its effect on classifier accuracy, in *Classif. Clust. Data Min. Appl.* (Springer, 2004) pp. 639–647.
- [66] W.-C. Lin and C.-F. Tsai, Missing value imputation: a review and analysis of the literature (2006–2017), *Artif. Intell. Rev.* **53**, 1487 (2020).
- [67] Q. Song and M. Shepperd, Missing data imputation techniques, *Int. J. Bus. Intell. Data Min.* **2**, 261 (2007).
- [68] Y. Zhou, S. Aryal, and M. R. Bouadjenek, Review for handling missing data with special missing mechanism, *arXiv preprint arXiv:2404.04905* (2024).
- [69] P.-R. Vlachas, J. Pathak, B. R. Hunt, T. P. Sapsis, M. Girvan, E. Ott, and P. Koumoutsakos, Backpropagation algorithms and reservoir computing in recurrent neural networks for the forecasting of complex spatiotemporal dynamics, *Neural Netw.* **126**, 191 (2020).
- [70] C. M. Bishop, Training with noise is equivalent to Tikhonov regularization, *Neural Comput.* **7**, 108 (1995).
- [71] S. Hochreiter and J. Schmidhuber, Long short-term memory, *Neu. Comp.* **9**, 1735 (1997).